The Plant Cell, Vol. 16, 2463–2480, September 2004, www.plantcell.org © 2004 American Society of Plant Biologists

# The SHINE Clade of AP2 Domain Transcription Factors Activates Wax Biosynthesis, Alters Cuticle Properties, and Confers Drought Tolerance when Overexpressed in Arabidopsis [W]

**Asaph Aharoni,[a] Shital Dixit,[a] Reinhard Jetter,[b] Eveline Thoenes,[a] Gert van Arkel,[a] and Andy Pereira[a,1]**

[a] Plant Research International, 6700 AA, Wageningen, The Netherlands
[b] Departments of Botany and Chemistry, University of British Columbia, Vancouver, British Columbia, Canada V6T 1Z4

**The interface between plants and the environment plays a dual role as a protective barrier as well as a medium for the exchange of gases, water, and nutrients. The primary aerial plant surfaces are covered by a cuticle, acting as the essential permeability barrier toward the atmosphere. It is a heterogeneous layer composed mainly of lipids, namely cutin and intracuticular wax with epicuticular waxes deposited on the surface. We identified an *Arabidopsis thaliana* activation tag gain-of-function mutant *shine* (*shn*) that displayed a brilliant, shiny green leaf surface with increased cuticular wax compared with the leaves of wild-type plants. The gene responsible for the phenotype encodes one member of a clade of three proteins of undisclosed function, belonging to the plant-specific family of AP2/EREBP transcription factors. Overexpression of all three *SHN* clade genes conferred a phenotype similar to that of the original *shn* mutant. Biochemically, such plants were altered in wax composition (very long fatty acid derivatives). Total cuticular wax levels were increased sixfold in *shn* compared with the wild type, mainly because of a ninefold increase in alkanes that comprised approximately half of the total waxes in the mutant. Chlorophyll leaching assays and fresh weight loss experiments indicated that overexpression of the *SHN* genes increased cuticle permeability, probably because of changes in its ultrastructure. Likewise, *SHN* gene overexpression altered leaf and petal epidermal cell structure, trichome number, and branching as well as the stomatal index. Interestingly, *SHN* overexpressors displayed significant drought tolerance and recovery, probably related to the reduced stomatal density. Expression analysis using promoter-β-glucuronidase fusions of the *SHN* genes provides evidence for the role of the *SHN* clade in plant protective layers, such as those formed during abscission, dehiscence, wounding, tissue strengthening, and the cuticle. We propose that these diverse functions are mediated by regulating metabolism of lipid and/or cell wall components.**

## INTRODUCTION

Plant surfaces are protected by a heterogeneous lipid polyester layer, consisting of cutin or suberin, that is codeposited with waxes. Cutin is the major component of the cuticle that overlays the cell walls of epidermal cells and forms the protective tissue on primary aerial organs. The functionally related suberin is an extracellular matrix that seals off particular layers of a plant and also strengthens specific tissues. Waxes are most evident in the form of epicuticular crystals that are exposed on the surface of certain organs and species but are also embedded as intracuticular waxes within the polymer matrix of cutin (Jetter and Schaffer, 2001) and suberin.

The cutin biopolyester is composed mainly of interesterified hydroxy and epoxy-hydroxy fatty acids, 16 and 18 carbons in length (Nawrath, 2002). The suberin polymer is composed of aliphatic chains (e.g., ω-hydroxy fatty acids, 16 to 28 carbons and α,ω-fatty diacids, 16 to 26 carbons), phenolic components (e.g., CoA esters or alcohols derived from hydroxycinnamic acids), and glycerol (Moire et al., 1999). Wax most often consists of homologous series (>18 carbons in length, typically 24 to 34) of saturated, straight very-long-chain fatty acids (VLCFAs), alcohols, aldehydes, alkanes, ketones, and esters (Kunst and Samuels, 2003).

The cuticular layer, comprising cutin and waxes, plays multiple roles in plants, including the regulation of epidermal permeability and nonstomatal water loss and protection against insects, pathogens, UV light, and frost (Sieber et al., 2000). In addition, it also functions in normal plant developmental processes, including the prevention of postgenital organ fusion and pollen–pistil interactions. It has been suggested that cuticle permeability in such processes will also influence cell-to-cell communication by enhancing or attenuating the passage of signal molecules (Pruitt et al., 2000; Sieber et al., 2000). Such signals could be required, for example, for organ adhesion (moving across the cuticle) or for mediating signaling between trichomes and stomata (moving within the developing epidermis) (Lolle et al., 1997; Krolikowski et al., 2003). The functionally

[1] To whom correspondence should be addressed. E-mail andy.pereira@wur.nl; fax 31-0317-418034.
The author responsible for distribution of materials integral to the findings presented in this article in accordance with the policy described in the Instructions for Authors (www.plantcell.org) is: Andy Pereira (andy.pereira@wur.nl).
[W] Online version contains Web-only data.
Article, publication date, and citation information can be found at www.plantcell.org/cgi/doi/10.1105/tpc.104.022897.

related suberin also prevents water loss from specific tissues, blocks pathogen invasion, and strengthens the cell wall. Apart from constitutive deposition of suberin, as for example in root endodermis, in the abscission zone during seed development, and in secretory organs, it is also deposited upon wounding (Kolattukudy, 1981; Nawrath, 2002).

The precursors for the synthesis of cutin, wax, and the aliphatic monomers of suberin are derived from plastidic de novo fatty acid synthesis, which generates palmitic (16:0), stearic (18:0), and oleic (18:1) acid attached to acyl carrier protein. Part of these precursors are then cleaved from acyl carrier protein by thioesterases and exported to the endoplasmic reticulum as fatty acyl-CoAs (Schnurr et al., 2004). At this point, the pool of acyl-CoAs is split to various metabolic pathways, including the synthesis of membrane lipids, seed storage lipids, and cuticular lipids. In the case of wax biosynthesis, stearic acid ($C_{18}$) acyl-CoAs are predominantly used for generating VLCFAs through sequential additions of two carbon units in a reaction catalyzed by membrane-bound, multienzyme acyl elongase systems. The VLCFAs formed could either be hydrolyzed to free fatty acids, reduced to aldehydes that are further derivatized to alkanes, secondary alcohols, and ketones (in the decarbonylase pathway), or used for the generation of wax esters by condensing primary alcohols (derived from reduced aldehydes) with free fatty acids (in the acyl reduction pathway; Millar et al., 1999). Monomers of cutin, on the other hand, are synthesized from the 16:0 and 18:1 fatty acyl-CoAs by multiple hydroxylation and epoxidation reactions (Kolattukudy, 1981) in which cytochrome P450-dependent enzymes are primary candidates to be involved. It was suggested that biosynthesis of cutin monomers will also involve lipoxygenases, peroxygenases, and epoxides (Blee and Schuber, 1993) and that the cutin polymer is formed by linking CoA-bound monomers to free hydroxyl groups in the polymer, a reaction catalyzed by acyl-CoA:cutin transferase (Reina and Heredia, 2001). Suberins and cutins are closely related in structure but differ in chain length and substitution patterns of their fatty acids, as in contrast with cutin, suberin contains a lignin-like domain (i.e., hydroxycinnamic acid derivatives) and glycerol. After elongation of the fatty acid carbon chain (as in wax biosynthesis), the oxidation of fatty acids to ω-hydroxy fatty acids was suggested to be catalyzed by cytochrome P450-dependent enzymes. The next step to form α,ω-fatty diacids could be executed either by the activity of the same cytochrome P450 or by dehydrogenases (LeBouquin et al., 2001; Nawrath, 2002).

Reduction of epicuticular crystals on stems of *Arabidopsis thaliana*, caused by compositional changes or reduced wax load, are relatively easy to detect, and this facilitated the identification of mutant lines, most of them (termed eceriferum [*cer*] mutants) described by Koornneef et al. (1989) and by McNevin et al. (1993). Several *cer* mutants were affected in fertility under low humidity because of defective lipid-rich pollen coat. Mutants altered in leaf cuticular waxes were also described in Arabidopsis and other species, including sorghum (*Sorghum bicolor*), maize (*Zea mays*), broccoli (*Brassica oleracea*), and pea (*Pisum sativum*) (Jenks et al., 1996). Many genes associated with cuticular wax metabolism in Arabidopsis were isolated and characterized. *CER1* has been proposed to encode an aldehyde decarbonylase (Aarts et al., 1995) mainly because of the increase in aldehydes and reduced levels of alkanes, secondary alcohols, and alkanes in the *cer1* mutant. The *CER2* gene might code for a CoA-dependent acyltransferase, but its precise function is unknown (Negruk et al., 1996; Xia et al., 1996; Kunst and Samuels, 2003). The *cer2* mutant accumulates C26 and C28 acyl groups, primary alcohols, and wax esters and shows reduced levels of the decarbonylation pathway products. The function of *CER3* is also not clear, and recent database searches showed that it might encode an E3 ubiquitin ligase, which is part of the ubiquitination-proteosome pathway (Kunst and Samuels, 2003). Several genes playing a role in the fatty acid elongation pathway that generate VLCFA wax precursors also have been characterized. They include the *FATTY ACID ELONGATION1* homologs (James et al., 1995), *3-KETOACYL-CoA SYNTHASE* (Todd et al., 1999), *FIDDLEHEAD* (*FDH*; Yephremov et al., 1999; Pruitt et al., 2000), *CUT1*/*CER6*, and *CER60* (Millar et al., 1999; Fiebig et al., 2000). Hooker et al. (2002) suggested that because of its very broad expression (throughout all stages of stem and leaf development and in the inflorescence), CER6 is the key condensing enzyme for wax biosynthesis in Arabidopsis, whereas other enzymes expressed very specifically mediate temporal need for increase in wax production.

Recent reports have also provided insights into the metabolism of cutin in plants. Chen et al. (2003) reported the isolation of the *WAX2* gene and interpreted it to be required for both cutin and cuticular wax deposition. The cuticular membrane of *wax2* weighed less and was thicker, disorganized, and less opaque. The total wax load on leaves and stems was decreased to 20%, showing a reduction in the decarbonylase pathway products and an increase in the acyl reduction pathway products. The WAX2 protein shows 32% similarity to CER1 and contains certain regions with homology to sterol desaturases and short-chain dehydrogenases/reductases. It was suggested that it plays a metabolic role in both cutin and wax synthesis and therefore points to a link between cutin and wax metabolism. The cloning and characterization of the same gene (*YRE*) was described by Kurata et al. (2003), who suggested that it might encode an enzyme catalyzing the formation of aldehydes in the decarbonylation pathway. Long-chain acyl-CoA synthetases (LACS) play a role in fatty acid metabolism and transport of fatty acids between cellular compartments. Schnurr et al. (2004) investigated the *LACS2* gene and suggested that it might act in the synthesis of cutin or cuticular wax in young expanding tissues and the epidermal layers of leaves. The recombinant LACS2 protein could very efficiently activate 16-hydroxypalmitate, an intermediate in the pathway to cutin synthesis. The *lacs2* mutant cuticle was thinner than the wild type and showed several pleiotropic effects, such as reduced leaf size and plant growth and reduced seed production and germination rates. The Arabidopsis *LACERATE* gene (*LCR*; Wellesen et al., 2001) encodes a cytochrome P450 of the CYP86 family and was also implicated in the epidermal biosynthesis of cutin. Enzyme activity assays using the recombinant LCR protein showed that it could efficiently catalyze the formation of ω-hydroxy fatty acids (ranging from C12 to C18:1). *LCR* is predominantly expressed in the inflorescence and siliques and also in roots and young seedling tissue, and it is the first cytochrome P450 ω-hydroxylase for

which a mutant has been isolated. The *lcr* mutant phenotype shows various developmental abnormalities such as postgenital organ fusions and effects on cell differentiation. Another mutant that shows cuticular defects is the *abnormal leaf shape1*, which shows defective cuticle in embryos and juvenile plants, and the corresponding gene encodes a subtilisin-like Ser protease (Tanaka et al., 2001). It is clear from the set of mutants characterized up to date that an intact cutin layer is needed for normal epidermal differentiation and organ formation as was exemplified by Sieber et al. (2000) in transgenic plants expressing a fungal cutinase.

Using activation tagging, we have isolated and characterized an Arabidopsis mutant, *shine* (*shn*) displaying characteristics of plant surface defects. Compared with the wild type, leaves of *shn* show a deep shiny green appearance, with curled structure, and also are altered in cuticle permeability, cuticular wax load/structure, and epidermal differentiation. The *SHN* gene encodes an AP2/EREBP transcription factor, and the characterization of two of its homologs, including detailed analysis of their expression patterns, suggests that this clade of genes acts in the regulation of lipid biosynthesis required for protection of plants to the environment, including organ separation processes and wounding.

## RESULTS

### Identification of the *shn* Mutant

By screening a collection of 2000 transposon activation tag lines (Marsch-Martinez et al., 2002), a mutant plant was identified that showed leaf surface alterations (Figure 1A). Both rosette and cauline leaves of the mutant (termed *shn*) had a more brilliant, shiny green color when compared with wild-type plants and often had curved-down edges (Figure 1A). The stem of mature plants was often bowed down and siliques were slightly smaller than the wild type and also showed a more brilliant surface. Structure of other floral organs and plant fertility did not seem to be affected in *shn*. Progeny analysis of the self-pollinated *shn* mutant line suggested a dominant mutation (three-quarters of the plants exhibited the *shn* phenotype).

### Alterations to Wax Load and Cuticle Permeability in the *shn* Mutant

We used scanning electron microscopy for a detailed comparison between the surfaces of wild-type plant organs and those of *shn*. The surfaces of stems and siliques of Arabidopsis are covered by a dense mixture of different types of wax crystals, whereas leaf surfaces normally exhibit only small numbers of epicuticular wax crystals. In contrast with the wild type, we detected more wax crystals on both adaxial and abaxial sides of rosette and cauline leaves of *shn* (Figure 2). The leaf surface was not entirely covered by crystals, as in the case of wild-type siliques and stems, but rather had irregular patches of plate-like wax crystals. An additional characteristic of the *shn* mutant was the presence of cuticular ridges on the surface of both cauline leaves and siliques, which were not detected in the wild type (Figure 2). Such cuticular ornamentation was not visible on either the adaxial or abaxial surfaces of *shn* rosette leaves. Freeze fractionation of siliques and cauline leaf tissues further demonstrated the presence of the cuticular ridges in *shn* tissues, which showed similarity to the cuticular ridges present normally on surfaces of wild-type Arabidopsis petals (Figure 2). In this analysis, the cuticle thickness did not seem to be drastically altered. Neither an increase in wax crystal numbers nor cuticular ridges were detected on surfaces of *shn* sepals, anther filament, and petals.

We conducted a detailed chemical analysis of total wax mixtures in both *shn* and wild-type leaf cuticles to quantify the changes in wax load detected by scanning electron microscopy. The *shn* mutant wax phenotype was characterized by a sixfold increase in wax coverage over the wild type, expressed as mass of extractable cuticular lipids per surface area (Table 1). Wild-type leaf wax was found to contain approximately equal amounts of compounds from the acyl reduction pathway (primary alcohols and alkyl esters) and from the decarbonylation pathway (alkanes, secondary alcohols, and ketones). By sharp contrast, the *shn* mutant wax was characterized by differences in amounts of compounds resulting from both pathways. Whereas primary alcohols and alkyl esters showed only 2.8- and 1.4-fold increases, the alkanes, secondary alcohols, and ketones were increased by 9.0-, 11.9-, and 11.0-fold, respectively. Aldehydes, regarded as intermediates of the decarbonylation pathway, showed 2.2-fold higher levels in the mutant wax mixture. Similarly, other compound classes (fatty acids, branched alcohols, and steroids) were also found at elevated levels in the mutant wax, albeit only with moderate increases.

In both wild-type and mutant leaf waxes the fatty acids, aldehydes, and primary alcohols were dominated by constituents with even carbon numbers, as expected for acyl derivatives resulting from $C_2$ elongation cycles (Figure 3). The alkanes, secondary alcohols, and ketones showed a clear preponderance of odd-numbered representatives, typical for metabolites from the elongation/decarbonylation route. The wild-type wax showed chain length distributions dominated by $C_{32}/C_{34}$ for fatty acids and aldehydes, by $C_{31}$ for alkanes, and by $C_{26}/C_{28}$ for primary alcohols. Only $C_{29}$ secondary alcohol and ketone, with functional groups both in the $C_{14}$ and $C_{15}$ position, could be detected. As compared with these wild-type patterns, the mutant leaf wax contained much higher concentrations of $C_{30}$ fatty acid, $C_{30}$ aldehyde, and $C_{27}/C_{29}$ alkanes, compensating for lower relative amounts of $C_{34}$ fatty acid, $C_{34}$ aldehyde, and $C_{33}$ alkane, respectively (Figure 3). The chain length distribution of secondary alcohols, ketones, and primary alcohols were similar in the wild type and the mutant.

To investigate whether the *shn* cuticular membrane properties were also altered, we conducted a chlorophyll leaching experiment in which rosette leaves from both *shn* and wild-type plants were submerged in 80% ethanol for different time periods, and the chlorophyll concentration in the solution was determined. Chlorophyll was extracted much faster from leaves of *shn* leaves as compared with the wild type (Figures 1B and 1C); therefore, the higher elution of chlorophyll from *shn* leaves indicates an increase in cuticle permeability.

To assay cuticular water loss, we monitored fresh weight changes of detached rosettes. Roots and emerging

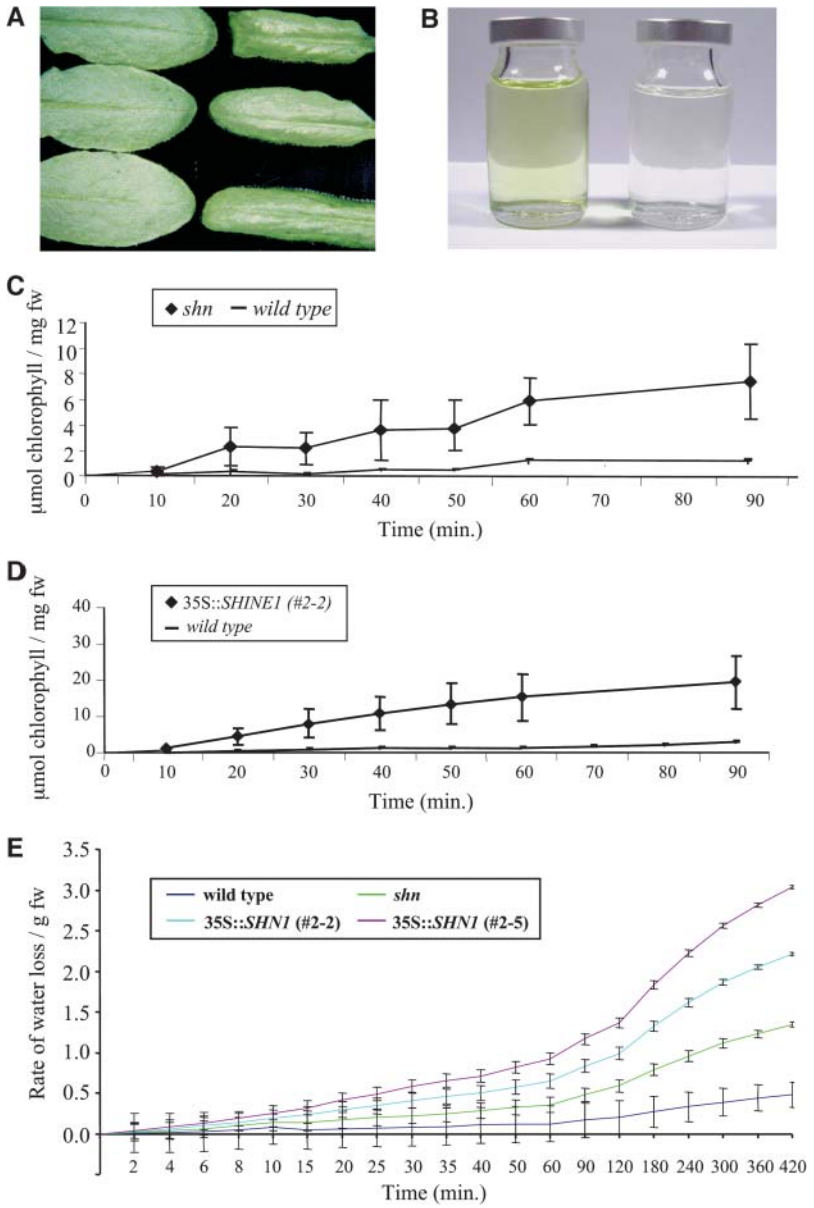


**Figure 1.** The *shn* Mutant and 35S:*SHN1*/*WIN1* Plants Phenotype and Surface Permeability.

**(A)** Mature rosette leaves of wild-type plants (ecotype Wassilewskija [Ws]) and the *shn* activation tag mutant on the left and right, respectively.
**(B)** Chlorophyll extracted in 80% ethanol for 1 h from mature rosette leaves of *shn* progeny (left container) compared with wild-type leaves (right container).
**(C)** Chlorophyll leaching assays with mature rosette leaves of *shn* and wild-type immersed in 80% ethanol for different time intervals. The results are derived from three independent experiments and depicted with standard error of the mean for each time point. fw, fresh weight.
**(D)** Chlorophyll leaching assays as described above but using mature rosette leaves derived from 35S:*SHN1*/*WIN1* (2-2) progeny and wild-type plants.
**(E)** Rate of water loss from the progeny of the activation tag *shn* mutant, two 35S:*SHN1*/*WIN1* primary transformants (2-2 and 2-5), and the wild type. Four rosette explants (root system and inflorescence stem detached) were weighed during the time intervals depicted. The results are derived from three independent experiments and depicted with standard error of the mean for each time point.

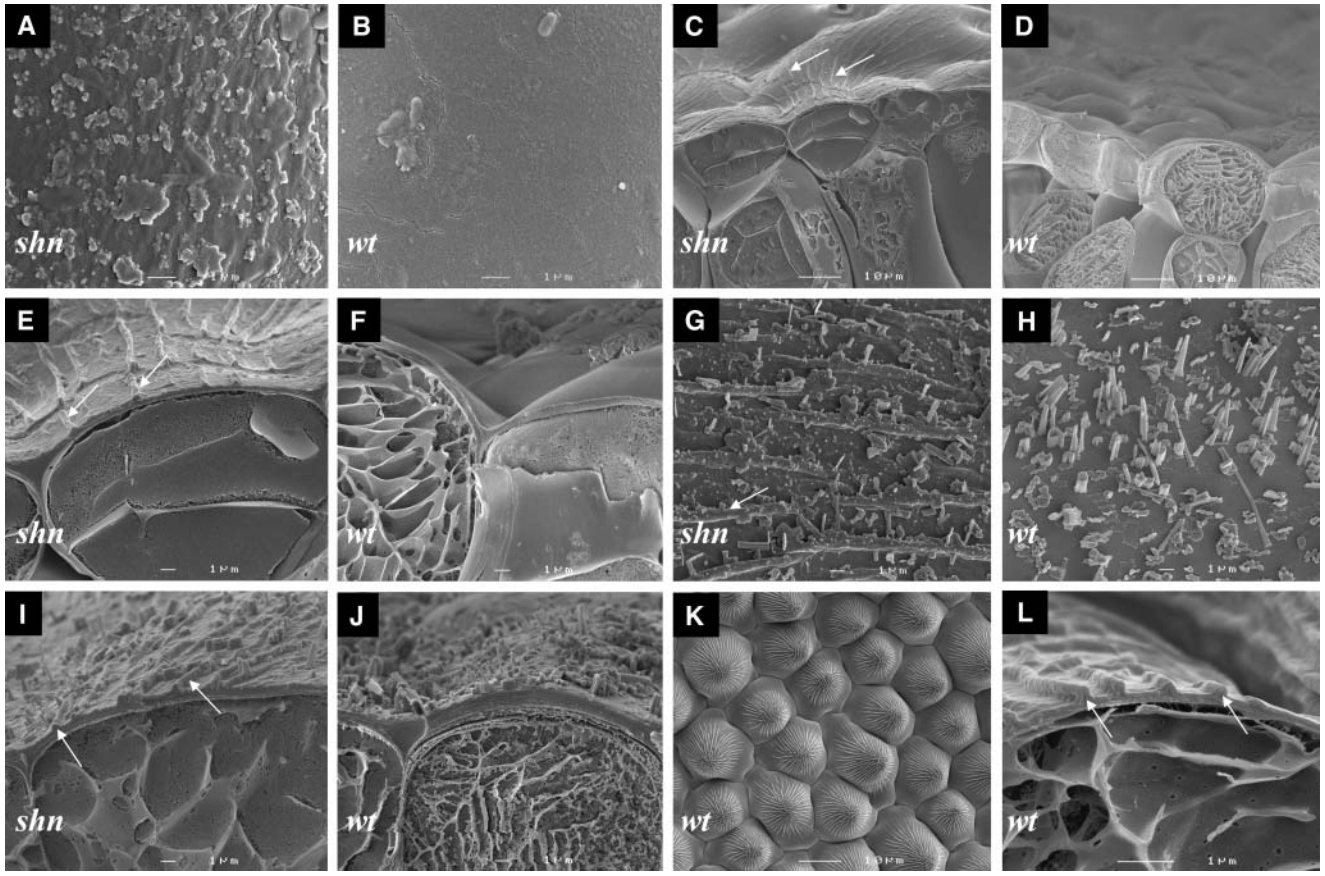


**Figure 2.** Changes in Wax Load and Surface Ornamentation of the *shn* Mutant Detected by Scanning Electron Microscopy.

**(A)** and **(B)** Images of *shn* and wild-type mature adaxial side rosette leaves, respectively. Surface of *shn* is covered with regions of wax deposition, whereas wild-type surface is smooth and shows only little wax deposition.

**(C)** and **(D)** Images of *shn* and wild-type cauline leaves after freeze fractionation, respectively. Cuticular ridges (indicated by arrows) could be detected on the surface of *shn*, whereas the wild-type surface is smooth.

**(E)** and **(F)** Enlarged images of **(C)** and **(D)**. Arrows point to the cuticular ridges in *shn*.

**(G)** and **(H)** Images of silique surface derived from *shn* and wild-type plants, respectively. The surface of *shn* contains long ridges (indicated by an arrow) apart from wax crystals, whereas surface of the wild type is covered only by wax crystals.

**(I)** and **(J)** Images of siliques after freeze fractionation derived from *shn* and the wild type, respectively. Cuticular ridges (depicted with arrows) could be detected on the surface of *shn* but not on the wild-type surface.

**(K)** An image of the wild-type adaxial petal surface covered with conical cells containing cuticular ridge ornamentation.

**(L)** An image of wild-type adaxial petal surface after freeze fractionation in which the cuticular ridges in the previous image **(K)** are detected (arrows). Compare these ridges to those detected by freeze fractionation of cauline leaves and siliques of *shn* (**[C]**, **[E]**, and **[I]**).

inflorescence stem of 4-week-old seedlings were detached from the rosettes, which were used to examine loss of water over time. The results (Figure 1E) show that fresh weight loss from the rosette tissues was increased in *shn* when compared with wild-type rosette tissues. As this water loss in *shn* continues beyond the time when stomata close (Yoshida et al., 2002), it is the increased cuticular water loss in *shn* that is revealed.

### A Member of the AP2/EREBP Transcription Factor Family Is Responsible for the *shn* Mutant Phenotype

DNA gel blot analysis showed that *shn* contains a single insertion (data not shown). Isolation and sequence analysis of DNA flanking the insertion site further indicated that the insertion is located in an intergenic region on chromosome 1. As can be seen in Figure 4A, the location of the 35S enhancer tetramer is between a gene encoding an unknown protein (4025 bp upstream of the promoter) and a gene encoding a member of the plant-specific AP2/EREBP family of transcription factors (620 bp upstream of the promoter). To examine if these two genes were induced in expression in *shn* compared with the wild type, we conducted an RT-PCR experiment using cDNA isolated from *shn* and wild-type leaf tissues. The results showed that the genes from both sides of the 35S enhancer tetramer were induced in the *shn* mutant leaves compared with wild-type leaves (Figure 4B).

**Table 1.** Composition of Cuticular Wax on Leaves of the Wild Type and the *shn* Mutant

| Compound Class | Wild Type (Ws) ($\mu g/cm^2$) $n = 5$ | Mutant *shn* ($\mu g/cm^2$) $n = 7$ | Average Fold Increase |
|---|---|---|---|
| Fatty acids | 0.13 ± 0.02 | 0.50 ± 0.30 | 3.8** |
| Aldehydes | 0.05 ± 0.03 | 0.11 ± 0.12 | 2.2 |
| Primary alcohols | 0.18 ± 0.03 | 0.50 ± 0.28 | 2.8** |
| Alkyl esters | tr | 0.07 ± 0.05 | 1.4*** |
| Alkanes | 0.23 ± 0.06 | 2.08 ± 1.38 | 9.0*** |
| Secondary alcohols | tr | 0.10 ± 0.03 | 11.9*** |
| Ketones | 0.01 ± 0.01 | 0.11 ± 0.08 | 11.0*** |
| Steroids | 0.08 ± 0.05 | 0.34 ± 0.27 | 4.3** |
| Isoalcohols | 0.05 ± 0.04 | 0.11 ± 0.09 | 2.2 |
| Unidentified | 0.07 ± 0.07 | 0.84 ± 0.77 | 12.0 |
| Total | 0.80 ± 0.26 | 4.78 ± 2.35 | 6.0*** |

The coverage of total extracted lipids and of individual compound classes are given as mean values with standard deviation. tr, traces (<0.05 $\mu g/cm^2$ detectable). Level of significance obtained with a Student's *t* test are marked by the following: **, $P < 0.05$; ***, $P < 0.01$.

We chose the downstream gene (At1g15360), encoding the AP2/EREBP transcription factor, as our primary candidate determining the *shn* mutant phenotype. Consequently, the coding region of the gene (termed *SHN1* or *SHN1/WIN1*) was cloned and constitutively expressed in Arabidopsis under the control of the 35S promoter of *Cauliflower mosaic virus* (CaMV). In fact, all the transgenic plants raised (20 individuals) showed a phenotype resembling the original activation tag line, in particular the *shn* brilliant green leaf and silique surface and downward curling of the leaves (Figure 5A). The phenotype of most of the 35S:*SHN1/WIN1* lines (both primary transformants and subsequent generations) was more severe compared with the original *shn* mutant. In most cases, plants were smaller, and in some cases even dwarfed (3 to 5 cm in size upon maturity), and their leaves were strongly curved, even rolled (Figure 5B). Further chemical analyses showed that the transformant leaves had cuticular wax load, relative compositions of compound classes, and chain length distributions within these classes similar to the original *shn* activation tag mutant (data not shown).

In contrast with the activation tag *shn* mutant, flower morphology was also affected, particularly in petals that were folded and in part hidden between the sepals and the flower interior organs (Figures 5C and 5D). We also used scanning electron microscopy to investigate the surface petals derived from the *SHN1/WIN1* overexpressing lines (Figure 5E). The anterior and distal parts of the adaxial surface of wild-type Arabidopsis petals normally show a uniform spread of conical epidermal cells, which exhibit a typical cuticular ornamentation (Figures 5H and 2K). On the other hand, in *shn* petals, we could identify a mix of both typical, conical cells and much longer cells, often more than doubled in size (Figures 5F and 5G).

Changes in plant surface might lead to alteration in trichome characteristics; therefore, we analyzed the number and structure of trichomes in the first true leaves of 35S:*SHN1/WIN1* seedlings compared with the wild type. The adaxial side of the first true leaf of the wild type (ecotype Ws) contains ~25 of mainly triple-branched trichomes spread on its surface. By contrast, the first true leaves of 35S:*SHN1/WIN1* seedlings contained much lower numbers of trichomes, ranging from complete absence up to a maximum of 8 to 10 trichomes per leaves (Figures 5I and 5J). When trichomes were present on the first leaves of 35S:*SHN1/WIN1*, they were nearly all single branched and located on leaf blade margins. The same observations were also detected in leaves derived from older plants.

We tested whether two other features of epidermal cell differentiation were also altered by the overexpression of *SHN1/WIN1*. Both pavement cell density and stomatal density on the abaxial side of the 35S:*SHN1/WIN1* lines were reduced compared with wild-type leaves (Table 2). Calculating the stomatal index revealed that it was reduced by 41% in the 35S:*SHN1/WIN1* leaves compared with the wild type (Table 2).

Leaching assays with progeny of two 35S:*SHN1/WIN1* primary transformants (nos. 2-2 and 2-5) showed that their cuticle was more permeable to ethanol because chlorophyll could be extracted more easily (Figure 1D). In line with the overall stronger phenotype of the 35S:*SHN1/WIN1* lines, the difference in chlorophyll leaching compared with wild-type leaves was more dramatic than initially observed for the activation tag *shn* mutant (cf. Figures 1C and 1D). The two 35S:*SHN1/WIN1* primary transformants (nos. 2-2 and 2-5) also showed an increased rate of water loss compared with the wild type (Figure 1E).

### Overexpression of Two Other Members of the SHN Clade Results in a Similar Phenotype

The plant AP2/EREBP superfamily of transcription factors contains 141 members in Arabidopsis (Alonso et al., 2003). Sequence homology searches and phylogenetic analysis across the entire AP2/EREBP family showed that SHN1/WIN1 is part of a small, distinct group of three proteins, 199, 189, and 186 amino acid residues long (SHN1/WIN1, SHN2, and SHN3, respectively; Figure 6). They contain the highly conserved AP2 domain and

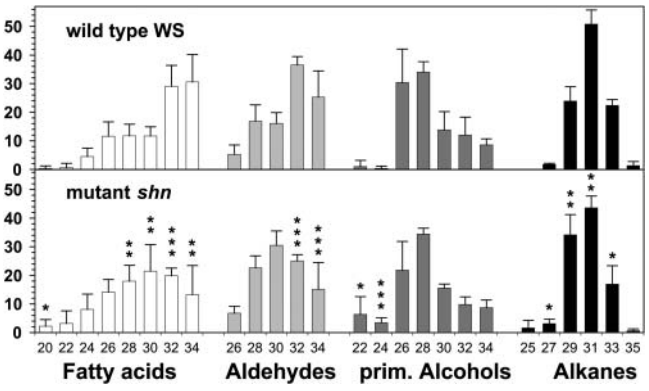


**Figure 3.** Chain Length Distribution (Percentage of Compound Class) for the Four Major Fractions in the Leaf Cuticular Wax of the Wild Type and *shn*.

Level of significance obtained with a Student's *t* test is marked by the following: *, $P < 0.1$; **, $P < 0.05$; ***, $P < 0.01$.

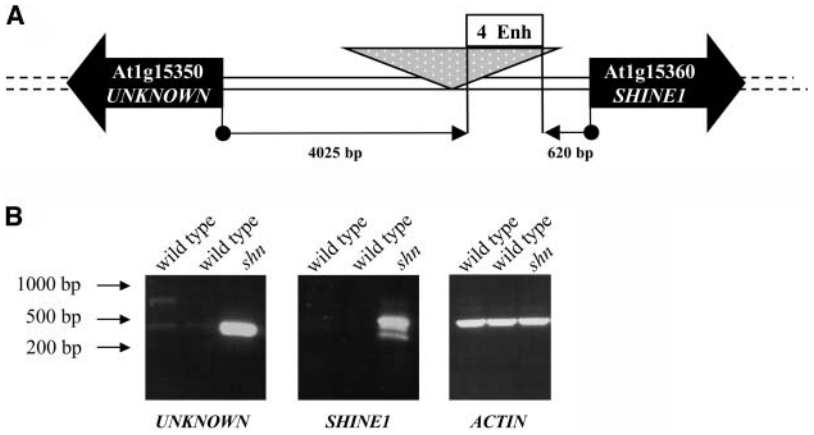


**Figure 4.** Location of the Transposon Insertion in the *shn* Mutant and Activation of the Flanking Genes.

**(A)** Location of the transposon insertion (inverted triangle) of *shn* on chromosome 1 between a gene with unknown function (At1g15350) and a member of the AP2/EREBP transcription factor family (At1g15360, *SHN1*). The distance of the enhancer (Enh) element in base pairs from the predicted ATG of the genes is also depicted.

**(B)** RT-PCR experiments using oligonucleotides for amplification of the two genes flanking the transposon insertion in *shn*. Expression of both genes is strongly induced in rosette leaves of *shn*, whereas hardly any signal could be detected in two different wild-type plants. Amplification of the actin gene was used as a control for presence and levels of cDNA.

share two other conserved motifs in their central portion (mm in Figure 6A) and C termini (cm in Figure 6A). The two complete motifs outside the AP2 domain are only present in the SHN clade proteins, whereas their next Arabidopsis homolog (At5g25190) contains only part of the mm domain and the cm domain (data not shown). SHN2 and SHN3 show the highest sequence identity among the three SHN proteins (71%), whereas SHN1 and SHN2 show the minimal homology among the clade members (55%). Interestingly, we could only identify a single protein sequence in the public database, from rice (*Oryza sativa*) (OsSHN1, accession number BAD15859), which contains the complete mm and cm regions and is most similar to the SHN clade proteins (showing 65% identity to SHN1; Figures 6A and 6B). In addition, the SHN clade members are conserved in gene structure because all three of them contain a single intron positioned 80 bp from the start codon. The *OsSHN1* gene contains a single intron that is located 3 bp further downstream (i.e., 83 bp of the first exon).

We reasoned that such sequence conservation outside the AP2 domain might associate the various SHN proteins to a similar functional role in Arabidopsis. Hence, the genomic regions encompassing the coding regions of *SHN2* and *SHN3* were used for overexpression (using the 35S CaMV promoter) of both genes in Arabidopsis plants. Interestingly, plants overexpressing *SHN2* and *SHN3* showed an identical visual phenotype to the one obtained when overexpressing the *SHN1/WIN1* gene, including the more brilliant, shiny green color of both rosette and cauline leaves, leaf curling, reduction in trichome number, and altered petal structure and silique length (Figures 6C and 6D).

### Spatial and Temporal Expression of the *SHN* Clade Members

To examine the expression of *SHN1/WIN1*, *SHN2*, and *SHN3*, we generated three plant transformation constructs, which linked 2.0-kb DNA sequences upstream of the predicted ATG codon of each gene to the β-*glucuronidase* (*GUS*) reporter gene. In general, GUS expression was detected in most plant organs, in some cases overlapping patterns were detected, whereas in others, very specific expression was evident in certain cell layers.

*SHN1/WIN1* expression was detected in the inflorescence and root tissues but not in stem, mature rosette leaves, or cauline leaves (Figure 7). Expression could be detected in sepals of very young closed buds (stage 6; Smyth et al., 1990) and later at stage 10. At that time, expression could also be detected in petals and developing gynoecium but not in stamens. In petals and sepals, veins were stained stronger than the rest of the organ, in which it was restricted to the epidermis. At anthesis (stage 13) the expression of *SHN1/WIN1* was reduced in the gynoecium, commenced in the anther, and showed weaker expression in the anther filament. When petals and sepals withered (stage 16), strong expression could be detected at the bottom of the silique, in the abscission zone, and in the pedicel region below it, whereas later, at silique maturity, it was detected in the same region but only at the nectaries. Additional GUS expression was observed at the branch points of pedicels of most young flowers in the inflorescence, in small lateral inflorescences (including the small bract adjacent to them), and in a patchy pattern in roots of mature plants and very young leaves in the rosette, including support cells of their trichomes.

The *SHN2* gene shows a pattern of expression associated with anther and silique dehiscence. At stage 12, when petals level with long stamens and tapetum degeneration is initiated in the anther (stage 10 of anther development; Sanders et al., 1999), expression could be detected in the stomium region. Up to anthesis, during which the septum is degenerated, a bilocular anther is formed, the stomium splits, and pollen is released, expression of *SHN2* became more specific to the dehiscence zone and continued until stamens fell off the senescing flower

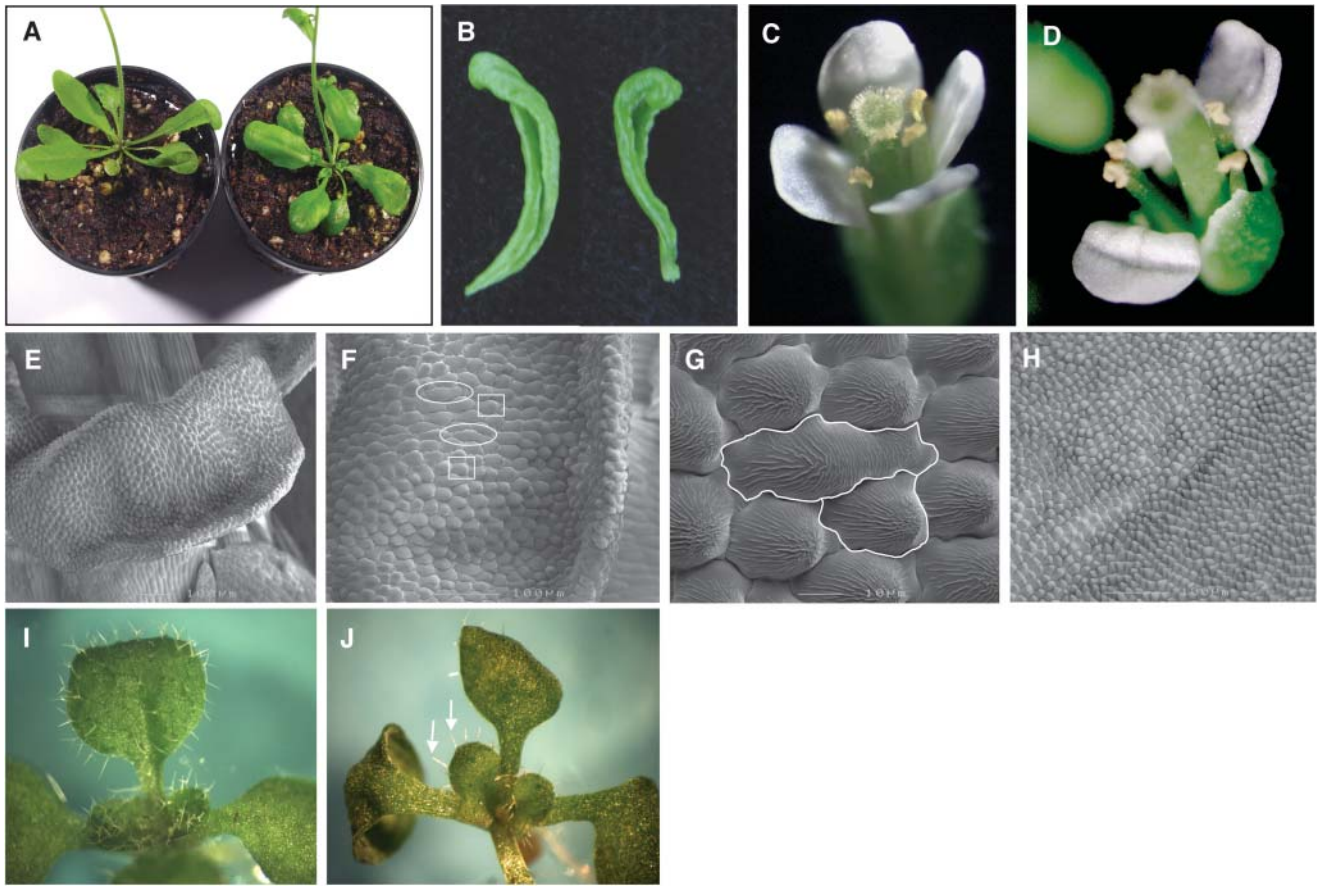


**Figure 5.** Recapitulation of the *shn* Mutant Phenotype and Detailed Morphological Changes in the 35S:*SHN1/WIN1* Lines.

**(A)** Rosette of wild-type and 35S:*SHN1/WIN1* line at the same age (on the left and right, respectively).
**(B)** Folded and twisted cauline leaves derived from a 35S:*SHN1/WIN1* line.
**(C)** and **(D)** A single flower of the wild type and 35S:*SHN1/WIN1* line, respectively, display the folding of petals in 35S:*SHN1/WIN1*.
**(E)** to **(G)** The adaxial surface observed using scanning electron microscopy of the distal part of a folded petal derived from a 35S:*SHN1/WIN1* flower. The surface is composed of typical petal epidermis conical cells (marked with a square in **[F]**) in addition to unusually longer cells more than twice the size of a typical cell (marked with an ellipse in **[F]**). Unusual and typical conical petal cells are marked in **(G)**.
**(H)** The adaxial surface of a distal part of a wild-type petal (at the same magnification shown in **[F]**) with typical conical cells detected.
**(I)** Seedling of a wild-type containing branched trichomes on the surface of its first and second pairs of true leaves.
**(J)** Seedling of 35S:*SHN1/WIN1* with hardly any trichomes on surface of first and second pairs of true leaves; the few detected are located on the blade margins and are single branched (marked with arrows).

(Figure 8). Subsequently, when petals and sepals withered (stage 16), GUS expression could be detected as an intense spot at the bottom of each valve. One stage later (i.e., in the growing phase of the green silique as it reached final length and the dehiscence zone differentiated), *SHN2* was strongly expressed along the valve margin-replum boundary, the region where pod shatter occurs, allowing seed dispersal.

The *SHN3* gene was most broadly expressed and was active in all plant organs. It showed expression in the vasculature and in the lateral root tip (Figure 9). When staining young 10-d-old seedlings, expression was detected in the support cells of trichomes present on the most newly formed leaves. In older leaves (rosette) as well as in cauline leaves, *SHN3* was mainly expressed in the central vein with lower expression in the entire blade. It was not expressed in a uniform manner in stems, showing mostly weak epidermal expression. Expression of *SHN3* in the inflorescence and young rosette leaves overlapped to a large extent with that observed for *SHN1/WIN1* (see above). Most interestingly, it showed an organ-specific wound induction. Although wounding did not induce it in rosette leaves, it did activate it in cauline leaves, stems, and siliques (Figures 9B and 9C).

The expression patterns we detected with GUS are supported by publicly available microarray data. Chen et al. (2002) analyzed the expression of 402 distinct transcription factor genes (including *SHN1* and *SHN3*) during multiple stages of Arabidopsis plant development and under various biotic and abiotic stresses. The data showed that *SHN2* is strongly and specifically expressed in

**Table 2.** Stomatal Density, Pavement Cell Density, and Stomatal Index of Mature 35S:*SHN1/WIN1* and Wild-Type Rosette Leaf Blades

| Plant Line | Stomatal Density (cells/mm$^2$ ± SD) | Pavement Cell Density (cells/mm$^2$ ± SD) | Stomatal Index |
|---|---|---|---|
| Wild Type | 27.03 ± 9.63 | 80.16 ± 19.88 | 25.22 ± 4.48 |
| 35S:*SHN1/WIN1* | 8.91 ± 3.76 | 51.56 ± 15.35 | 14.73 ± 3.96 |

flowers, whereas *SHN3* is expressed at similar levels in most Arabidopsis organs and is induced upon wounding. This corresponds to the expression patterns we detected in *SHN1* and *SHN3* promoter:GUS plants.

### Plants Overexpressing *SHN1/WIN1* Show Enhanced Drought Tolerance

We wanted to examine to what extent the change in plant surface, as a result from *SHN1/WIN1* overexpression, affected its drought tolerance capacity. To do so, 15-d-old seedlings of the original activation tag lines, two of the 35S:*SHN1/WIN1* transformant lines (line nos. 2-5 and 2-2), and the wild type (ecotype Ws) were exposed to a period of 9 to 11 d of dehydration (Figure 10). Subsequently, seedlings were watered and their recovery monitored for a week. Whereas wild-type plants did not recover from the dehydration treatments longer than 9 d and completely dried out, all seedlings derived from lines expressing the *SHN1/WIN1* gene recovered to become greener and stronger (Figure 10; see Supplemental Table 1 online). Consistent with the phenotype characteristics described above, seedlings derived from the activation tagged line were relatively weak in recovery when compared with the two transgenic 35S:*SHN1/WIN1* lines.

## DISCUSSION

In this study, we have identified and characterized a novel clade of AP2/EREBP transcription factors and showed that overexpression of either one of them will cause a major effect on the plant surface. Most if not all phenotypes that were detected by overexpressing the *SHN* genes have been described in other mutants (or transgenic lines) associated with epicuticular crystals or the cuticular membrane. As in the case of the *cer* stem mutants, and others including Arabidopsis leaf mutants (e.g., *wax1*; Jenks et al., 1996, 2002), the initial phenotype that made us notice *shn* was the bright, glossy appearance of the leaf surface.

The fact that in all *cer* mutants cuticular wax was decreased, whereas in *shn* it was increased, suggests that factors other than wax levels, possibly cuticular wax composition or alteration of the epidermal cells and overall surface structure, result in the *shn* glossy leaf surface phenotype. Indeed, rosette and especially cauline leaves were twisted and folded downwards, their surface appeared stretched, and their pavement cells were larger. When compared with the surface of wild-type petals, which normally exhibit a uniform plane of conical cells, petals of *SHN* overexpressors were also strongly wrinkled, possibly because of the presence of longer cells (often double in size or more) detected in their central and distal parts. Adding to this, the decrease in numbers of trichomes, changes in trichome branching patterns, and the alteration of stomatal indices emphasize that *SHN* genes strongly affect epidermal cell differentiation. Similarly, mutations in the *KCS* and *FDH* or *HIC* (Gray et al., 2000) genes result in alteration of stomatal density and trichome number, respectively. The *lcr* mutant showed a dramatically reduced trichome number, whereas *wax2/yre* had a reduction in stomatal index and reduced trichome size. Both *cer1* and *cer6/cut1* also showed an increase in stomatal index, whereas *lacs2* was altered in the shape of pavement cells. Thus, *shn* mutants substantiate the concept that composition of wax in the cuticle effects epidermal cell differentiation, possibly by mediating a transfer of signals for epidermal cell fate (Bird and Gray, 2003).

Some of the mutants described above showed different levels of postgenital fusions in which epidermal cells respond differently to physical contact with other epidermal cells, resulting in unification of primordial structures (Lolle et al., 1998). This anomalous feature occurs mainly during development of flower organs, as for example in the *fdh* mutant or in the transgenic lines expressing a fungal cutinase (Sieber et al., 2000). It is often accompanied by increased cuticle permeability, demonstrated by increased rates of chlorophyll extraction (Lolle et al., 1998). We could not detect signs of postgenital fusions in *SHN*-overexpressing lines, although the plants showed a dramatic increase in chlorophyll leaching when immersed in ethanol. This indicates that overexpression of *SHN* genes causes not only changes in epidermal differentiation but also structural defects in the cuticle, such as the ones detected by transmission electron microscopy surface analysis of *wax2*, *lacs2*, and the cutinase-expressing lines (all three also display increased chlorophyll leaching). Another point of evidence that plants overexpressing *SHN1/WIN1* are altered in the cuticular membrane was our fresh weight loss experiment. Rosette explants (without roots or inflorescence stem), derived either from *shn* or plants expressing *SHN1/WIN1*, showed a clear increase in water loss as compared with wild-type explants. Similar observations were reported for seedlings of *kcs-1* that were more sensitive to growth under low humidity conditions compared with the wild type (Todd et al., 1999), whereas Jenks et al. (2002) reported that some *cer* mutants lost water faster than the wild type. They did not find a clear relationship between cuticular wax load or composition and transpiration rates and therefore suggested a relation between the cuticular membrane structure (including intracuticular wax and cutin load and composition) and water transport.

The comparative chemical analyses of *shn* and wild-type leaf cuticular lipids revealed changes in both absolute wax levels and relative wax composition of the mutant. In absolute terms, *shn* caused a sixfold enhancement in total wax amount, to which all wax constituents contributed partially. In relative terms, the mutant wax composition was characterized by high proportion of alkanes, secondary alcohols, and ketones, whereas the chain length pattern within compound classes showed strong increases of $C_{30}$ fatty acid, $C_{30}$ aldehyde, and $C_{27}/C_{29}$ alkanes.

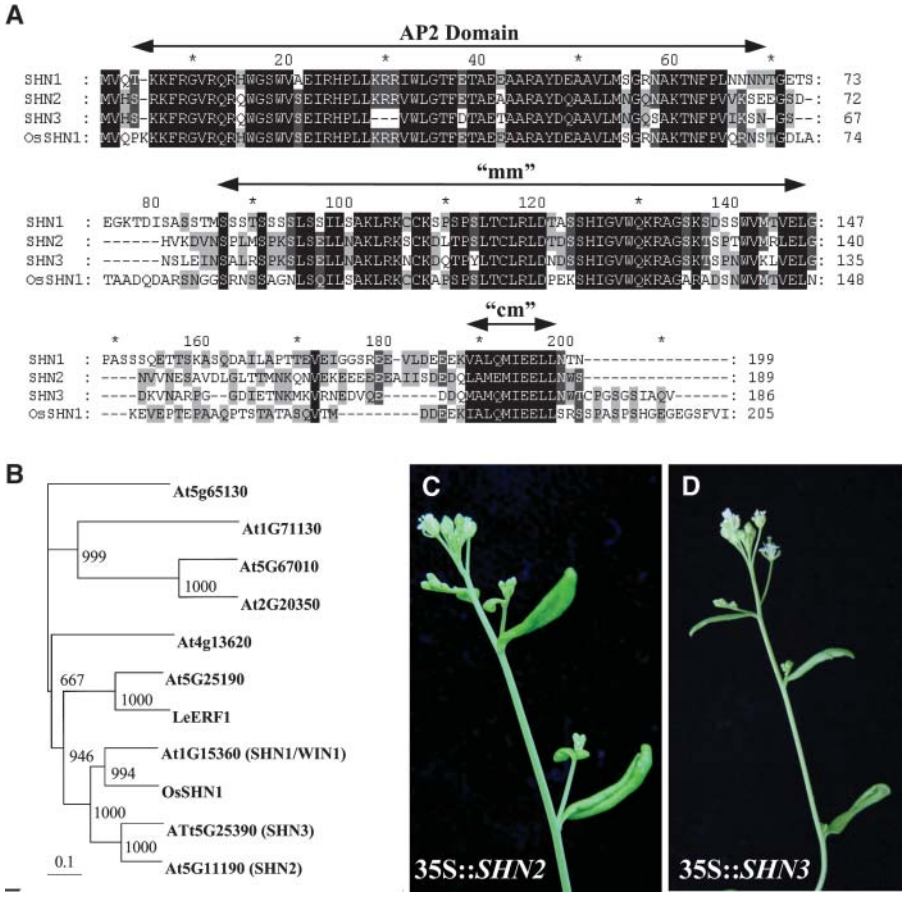


**Figure 6.** The SHINE Clade of the Arabidopsis AP2/EREBP Transcription Factor Family.

**(A)** Sequence alignment of the three Arabidopsis SHN proteins and their putative ortholog from rice (OsSHN1, accession number BAD15859). All four proteins contain a single AP2 domain at their N termini, a conserved middle domain (termed mm), and a conserved C-terminal domain (termed cm). Black background indicates 100% conservation, gray is 75%, and light gray is 50% conservation.

**(B)** Phylogenetic analysis of the SHN clade protein members and other closely related AP2/EREBP family proteins from Arabidopsis, tomato (*Lycopersicon esculentum*) (LeERF1, accession number AAL75809), and rice (OsSHN1, accession number BAD15859). The scale bar of 0.1 is equal to 10% sequence divergence. Bootstrap values are given for nodes and are considered as a value for significance of the branches. Values higher than 850 are likely to be significant.

**(C)** and **(D)** Plants overexpressing *SHN2* and *SHN3*, respectively. Note the characteristic twisted appearance of the cauline leaves.

Most strikingly, the mutant was characterized by especially high concentrations of products of the elongation/decarbonylation pathway of wax biosynthesis.

A synthesis of these results suggests that at least three separate regulative changes must be assumed to explain the role of SHNs in wax biosynthesis. First, this transcription factor seems to control genes responsible for early steps in the pathway, most likely the elongation steps leading from long-chain precursors to VLCFA. It is generally accepted that one or more β-ketoacyl-CoA synthases, with partially overlapping specificities for acyl-CoA precursor chain lengths between $C_{18}$ and $C_{22}$, are rate-limiting factors for this part of the pathway (Millar and Kunst, 1997). By upregulating the reaction capacity of this step, the *shn* mutant could cause an overall increase in quantities of all metabolic end products of wax biosynthesis. Second, *SHNs* likely also affect a later rate-limiting step in wax biosynthesis, thus causing shifts in relative portions of final products. The most drastic differences between wild-type and mutant wax were found in the relative increase of $C_{29}$ alkane, coinciding with the relative decrease of all compounds with chain lengths above $C_{30}$. Both the reduction/decarbonylation toward $C_{29}$ alkane and the elongation toward $C_{32}$ compounds share $C_{30}$ acyl-CoA ester as a direct precursor. The shift in relative portions of both product groups therefore suggests the differential regulation of both competing pathway branches by *SHNs* (i.e., of $C_{30}$ acyl-CoA reductase/decarbonylase versus $C_{32}$ β-ketoacyl-CoA synthase). Third, all products of the decarbonylation branch (i.e., $C_{29}$ alkane, secondary alcohol, and ketone) were found at proportionately increased levels in the mutant. Hence, the increased flux through the early elongation and decarbonylation steps must be processed by equally upregulated hydroxylation to the corresponding secondary alcohol

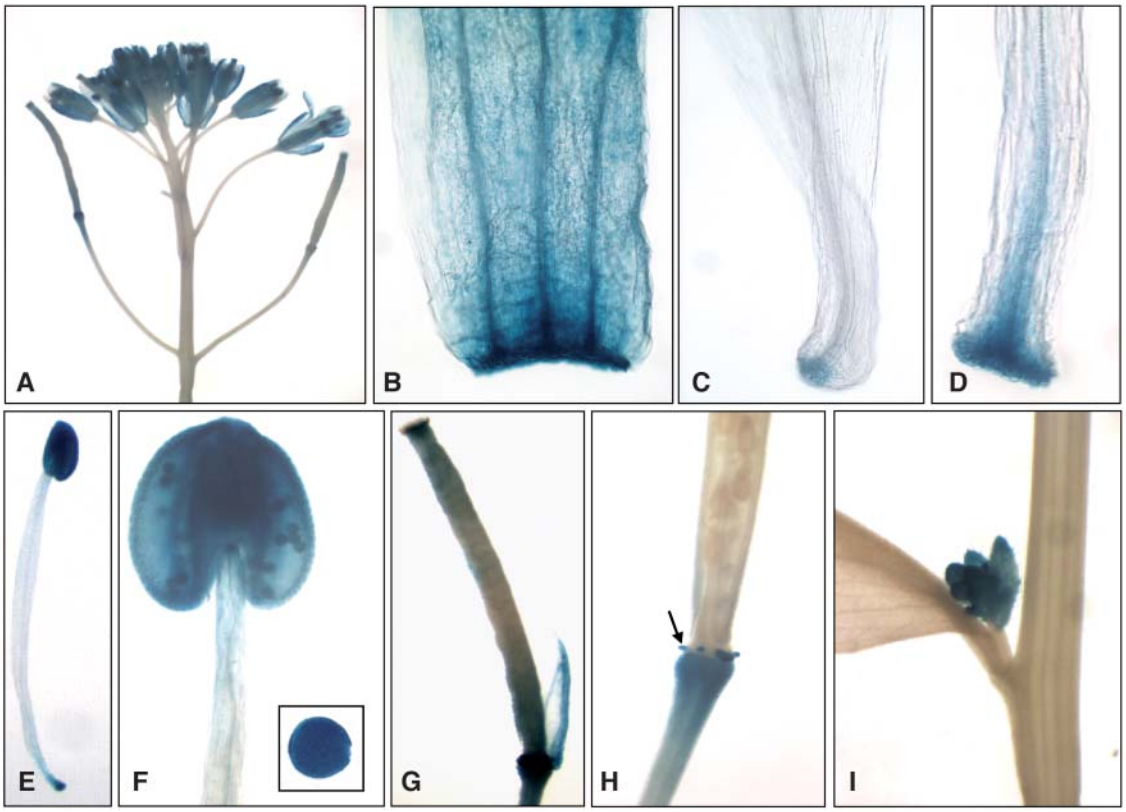


**Figure 7.** Expression Patterns of *SHN1/WIN1* Detected in *SHN1/WIN1* Promoter:GUS Lines.

**(A)** An inflorescence.
**(B)** Bottom half of a sepal.
**(C)** Bottom half of a petal.
**(D)** Bottom part of the stamen shown in **(E)**.
**(E)** A stamen.
**(F)** Top part of the stamen shown in **(E)** and the anther and a pollen grain (inset).
**(G)** Stage 16 silique.
**(H)** Stage 17 silique; the nectaries are marked with an arrow.
**(I)** An emerging lateral inflorescence.

and oxidation to the ketone. In summary, we hypothesize that the *shn* mutant is upregulated in early elongation, in the decarbonylation branch, and in the ensuing oxidation reactions, but not in the late elongation cycles beyond $C_{30}$. It is not clear at this stage whether the *SHN* genes act directly in the regulation of the three regulative alterations suggested above.

The SHN proteins are members of the plant superfamily of AP2/EREBP transcription factors that have been shown to act either in developmental programs, such as flower development, or as mediators in the plant responses to various environmental stresses (Okamuro et al., 1997; Liu et al., 1998; Riechmann and Meyerowitz, 1998; Singh et al., 2002). Different members of the AP2/EREBP family will regulate genes involved in response to pathogenesis, cold, drought, ethylene, and jasmonates (Memelink et al., 2001). Such response cascades could be executed by direct regulation of metabolic pathways, which lead to the production of metabolites essential for plant survival. An example of such activity was the identification of the *Catharanthus roseus* ORCA AP2/EREBP transcription factors, which activate the terpenoid indole alkaloid biosynthetic pathway as part of a methyl jasmonate–mediated response to stress. Two of the three members of the ORCA clade have been shown to bind to specific regions in promoters of overlapping but distinct sets of the terpenoid indole alkaloid pathway structural genes that contain a jasmonate- and an elicitor-responsive element in their promoters (Memelink et al., 2001). It is possible that the SHN clade members also act in a combinatorial manner to protect the plant internal and external layers from environmental influences, which might interact through common hormonal control systems, such as ethylene, abscisic acid, and jasmonates.

Several common characteristics of the SHN clade provide evidence that they are related in function. The first feature is the high similarity of the three proteins in terms of sequence, most notably outside the AP2 domain. The complete mm domain (Figure 6A) is only present in the Arabidopsis *SHN1/WIN1*, *SHN2*,

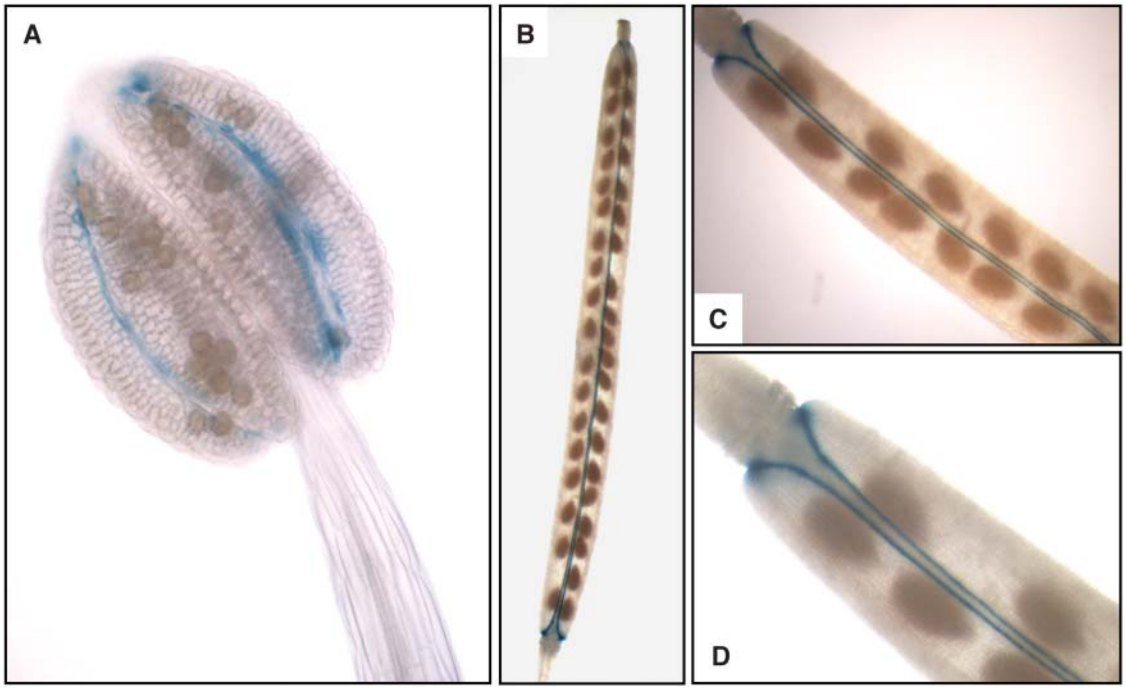


**Figure 8.** Expression Patterns of *SHN2* Detected in *SHN2* Promoter:GUS Lines.

**(A)** A dehiscing anther; dehiscence zone is stained blue.
**(B)** to **(D)** Mature silique at stage 17; dehiscence zone is stained blue.

and *SHN3* and in another single AP2/EREBP protein sequence in the public databases (the OsSHN1 protein from rice). OsSHN1, which was not yet associated with a function, might be the true ortholog of the Arabidopsis SHN proteins. The complete mm motif could therefore be an important common factor associated with SHN clade function. Adding to this is the well conserved gene structure among the three SHN proteins, including two exons and a single intron located at the same distance from the ATG start codon. A second common characteristic is that upon overexpression, all three proteins display the same phenotype. A similar observation was also reported recently for three members of the Arabidopsis *LATERAL ORGAN BOUNDARIES* family (Shuai et al., 2002), which upon overexpression under a constitutive promoter in Arabidopsis showed similar phenotypes (Nakazawa et al., 2003). Preliminary results with transgenic Arabidopsis plants overexpressing the nearest homolog of the SHN clade genes (At5g25190), under the control of the CaMV 35S promoter, did not show the typical morphological *shn* phenotype (data not shown). We suggest that the actual redundancy between the SHN factors is most probably in their target genes, but they differ in time and location of expression, which implies that they might play different roles both in normal conditions and under stress conditions.

Indeed, when analyzing expression of the three *SHN* clade members, we identified partial overlaps in terms of tissue specificity. In particular, the expression of *SHN1/WIN1* and *SHN3* overlaps, mainly in the inflorescence in the different flower organs, including the abscission zone at the bottom part of the silique. Expression of these two genes also appears similar in young growing leaves and leaf primordia (including their trichome support cells) and roots. On the other hand, we could not detect expression of *SHN1/WIN1* and *SHN2* in either stem or mature rosette or cauline leaves, whereas *SHN3* expression could be detected in these tissues. Expression of SHN2 is very specific, although we could detect some overlap in expression with *SHN3*, which showed faint expression all over the silique, including in the valve margin region where expression of *SHN2* was predominant. These similarities in expression might explain why we could not obtain loss-of-function phenotypes for any of the three *SHN* genes when attempting to obtain plants silenced for *SHN1/WIN1*, *SHN2*, and *SHN3* using the RNA interference approach (no knockout lines could be obtained to any of the genes in the public databases). However, in some cases, the very specific expression, as in the case of *SHN2*, could provide strong clues to gene function.

The most prominent link between the expression of all three genes, as detected by the GUS expression patterns, is the association with cell separation. Abscission and dehiscence are two main processes involving cell separation, and they facilitate pollen release from anthers, shedding of organs (including leaves, flower organs, seed, and fruit), and pod dehiscence. They usually involve a surgical procedure in which very specific layers are preprogrammed to differentiate differently from their surrounding cells (Roberts et al., 2002). Molecular evidence suggests that abscission and dehiscence encompass two major phases that involve cell-to-cell separation accompanied by

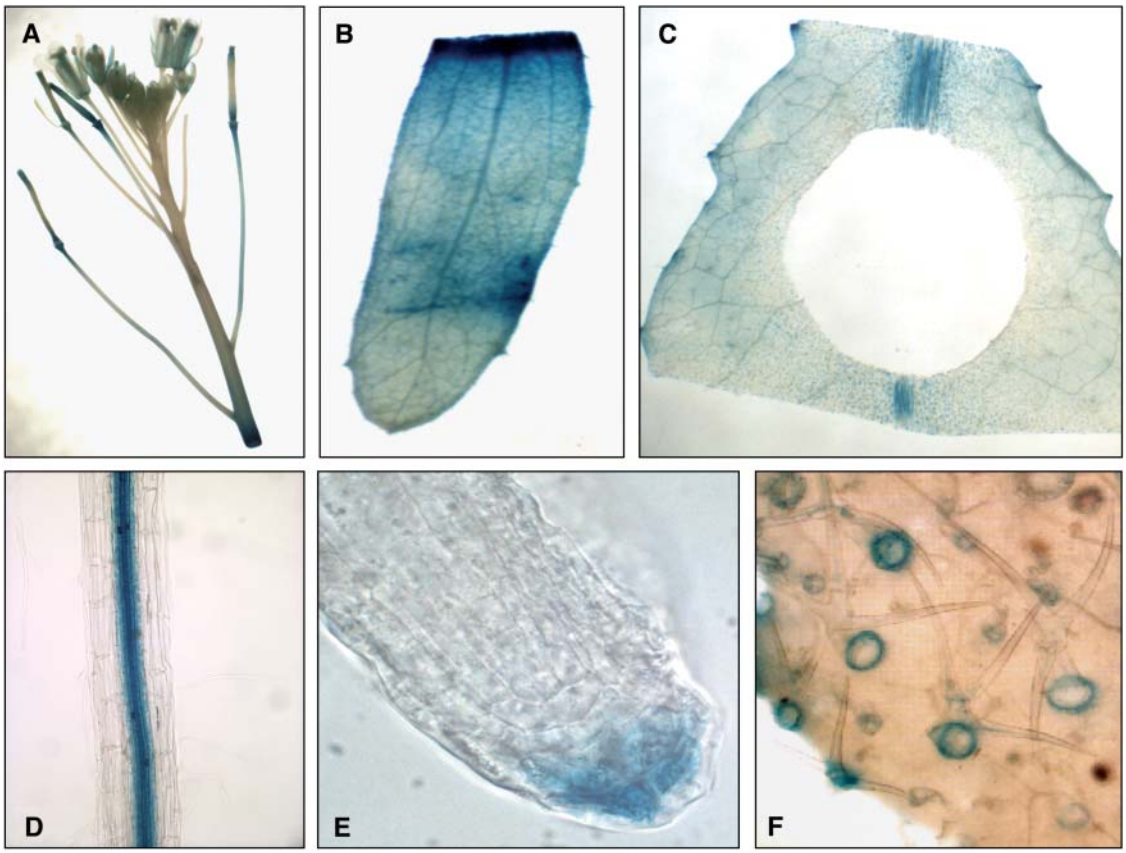


**Figure 9.** Expression Patterns of *SHN3* Detected in *SHN3* Promoter:GUS Lines.

**(A)** An inflorescence.
**(B)** Cauline leaf cut close to its proximal part with strong GUS staining at the cut edge.
**(C)** Rosette leaf with cut and wounded edges either inside (made by punching a disk in the blade) or at both sides of the leaf do not stain for GUS.
**(D)** Root of a 4-week-old plant grown in soil stained in the endodermis.
**(E)** Lateral root of a 4-week-old plant grown in soil stained in the root cap.
**(F)** Adaxial side of a young leaf derived from a 12-d-old seedling grown in vitro. Trichome support cells are stained blue.

protection of the cells by the formation of an anatomically different protective layer (Roberts et al., 2000). Such protective layers are formed both in the separating layers and at the areas surrounding them to shield against penetration of pathogens and to avoid desiccation. Suberin is very often deposited at the sites of protection, including upon wounding, which is a process most similar to cell separation events in which certain cell layers are damaged and require the formation of a physical barrier as part of their healing process (Kumar and Knowles, 2003). Shielding layers that include suberin deposition are also needed in roots when tissue damage occurs, in the root cap during penetration into the soil, or in the endodermis for the separation of the cortex from the central cylinder of the root, either as an apoplastic transport barrier or for protection from pathogens (Schreiber et al., 1999). Expression patterns of the three *SHN* clade members reveal localization and timing, which correspond with the process described above. These include strong expression in the layers of flower organs that go through abscission in *SHN1/WIN1*, highly specific and coordinated expression of *SHN2* in anther and silique dehiscence zones, and the expression of *SHN3* in root cap cells and the internal part of the root, including its induction by wounding. Expression of *SHN2* is especially interesting because it points to the fact that the two dehiscence processes occurring sequentially first in anthers and subsequently in siliques are coordinated by a similar regulatory circuit, and *SHN2* might be one of its elements. The expression patterns of the *SHN* genes emphasize a role in the interface between the outermost plant surfaces and the environment (wounding sites, root cap cells, and in some organs at the epidermal layers) and at the interface between cells and cell layers either above ground (e.g., the dehiscence and abscission zones) or below ground (e.g., the endodermis).

Cuticle metabolism and the structure of the epidermal surfaces are crucial factors in determining plant water management. To examine the effect of the different phenotypes we observed on drought tolerance, we conducted a set of experiments that

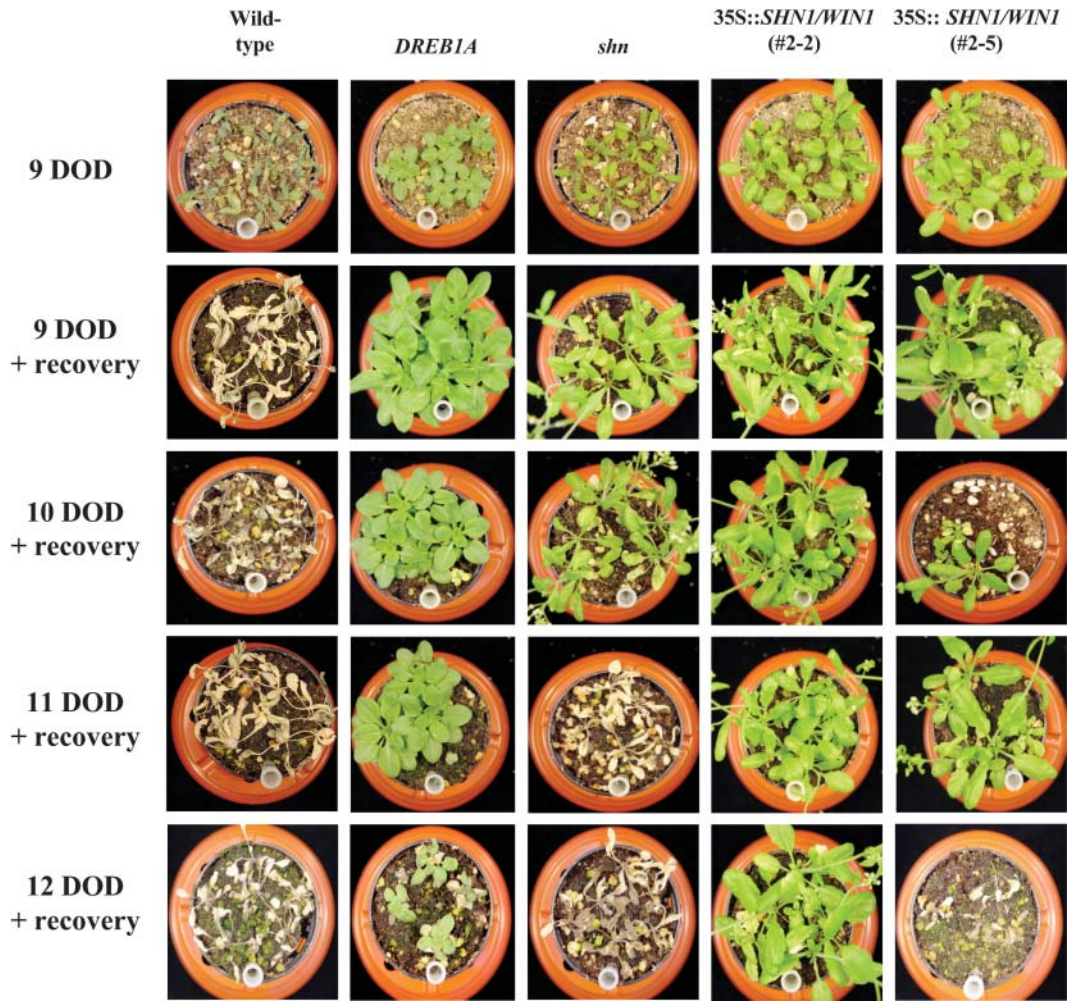


**Figure 10.** Drought Tolerance Experiment with *shn* and 35S:*SHN1/WIN1* Lines.

Fifteen-day-old seedlings (six seeds sown per pot) of the wild type, progenies of *shn*, two 35S:*SHN1/WIN1* lines (nos. 2-2 and 2-5), and a positive control rd29-DREB1A line (providing drought tolerance; Kasuga et al., 1999) were exposed for a period of 9 to 12 d of dehydration (DOD). Subsequently, seedlings were watered, and their appearance after a week (recovery) is presented in the image (apart from the first row at 9 d of dehydration, in which pictures were taken directly at the end of the dehydration period). The 9 d of dehydration results provide a clear difference between the wild type and *shn* as well as 35S:*SHN1/WIN1*, in which there is 100% recovery of the overexpression lines and 0% recovery of the wild type. Identical recovery results were obtained in an additional experiment comparing 50 seedlings of each wild-type and 35S:*SHN1/WIN1* (no. 2-5) lines. See also Supplemental Table 1 online. $n = 3$ in the comparison between 35S:*SHN1/WIN1* (no. 2-5) and $n = 2$ for all other comparisons.

demonstrated that overexpression of the *SHN* gene enhances the drought tolerance of the plant and its recovery after a period of water deficiency. Because a change in stomatal index was detected in plants overexpressing *SHN1/WIN1*, it is probable that the reduction in the number of stomata leads to reduced transpiration during the drought period. On the other hand, it cannot be ruled out that changes in the structure of the root system caused increased efficiency of the overexpression lines for uptake of water under water restriction. Preliminary visual observations performed on root systems of the wild type and overexpressors indicated a change in root structure with longer lateral roots in the overexpression lines. In this respect, it has previously been shown that plant stress and root growth conditions can alter root structure and components like suberin (Zimmermann et al., 2000).

This study identifies a novel clade of regulatory factors that influences the formation and metabolism of plant surfaces when overexpressed. Although the precise biological role of each *SHN* member has still to be determined, we suggest that each of them is required for the proper separation between cells, tissue layers, and the plant and its environment. Their function might therefore be to link the metabolism of lipid and/or cell wall components present in the cuticle or in internal plant interfaces to the coordinated execution of developmental programs in normal plant life or in response to environmental stresses.

## METHODS

### Plant Material and Drought Tolerance Experiment

All plants, including the activation tag population (Marsch-Martinez et al., 2002), and transgenic lines were grown in the greenhouse at ~22°C and were in the *Arabidopsis thaliana* ecotype Ws. For the drought tolerance experiments, soil mixture comprised one part of sand and perlite and two parts of compost (a mixture made up of 25% clay and 75% turf with EC = 1 [nitrogen, phosphorous, and potassium]; Hortimea, Elst, The Netherlands). Seeds were sown (after three nights at 4°C) at density of six plants per 4-cm pot in a tray with 51 pots (Aracon containers; BetaTech, Gent, Belgium). Nutrients (Hydroagri, Rotterdam, The Netherlands; 2.6 EC) were supplied 10 d after germination, and at 2 weeks after germination the plants were subjected to drought (for 9, 10, 11, or 12 d) by transferring the pots to dry trays (after drying each pot from outside). Every 2 d in drought, the plants were moved within the tray to nullify pot position effects. Subsequently, plants were rehydrated and observed for recovery after 1 week. Experiments comparing drought tolerance between the wild type and DREB1A, *shn*, and 35S:*SHN1/WIN1* (no. 2-2) plants were repeated twice and three times with 35S:*SHN1/WIN1* (no. 2-5) (see Supplemental Table 1 online).

### Isolation of Flanking DNA and Sequence Analysis

DNA was isolated according to Pereira and Aarts (1998) from two leaves or young flower buds, and 10 ng of genomic DNA was used for thermal asymmetric interlaced PCR as described by Marsch-Martinez et al. (2002). A re-PCR was generally performed before sequencing the amplified fragments and identifying the insert position in the Arabidopsis genome using a BlastN algorithm (Altschul et al., 1990) at the National Center for Biotechnology Information (http://www.ncbi.nlm.nih.gov). Multiple sequence alignments and phylogenetic analysis were performed using ClustalX 1.81 with default settings (Thompson et al., 1997). We used the neighbor joining method for calculating the phylogenetic tree and 1000 bootstrap replicates (recommended by the program). The GENEDOC (Nicholas et al., 1997) and TreeView (Page, 1996) programs were used for editing the alignment and drawing the phylogenetic tree, respectively.

### Generation of Plant Transformation Constructs and Transgenic Arabidopsis

Fragments encompassing the full-length coding regions were amplified (using *pfu* DNA polymerase) from flower buds cDNA (for *SHN1/WIN1*, At1g15360) or genomic *DNA* (for At5g11190, *SHN2* and At5g25390, *SHN3*) to generate the three overexpression constructs. The cDNA (produced as described below) and genomic DNA used for amplification were from the Arabidopsis ecotype Columbia. Oligonucleotides AP35 (5′-CGGATCCATGGTACAGACGAAGAGTTCAG-3′) and AP36 (5′-CGAGCTCGATTTAGTTTGTATTGAGAAGC-3′) were used to amplify *SHN1/WIN1*, whereas oligonucleotides AP69 (5′-CGGATCCATGGTACATTCGAGGAAGTTCCG-3′) and AP70 (5′-CGAGCTCTCAATCCAATTCAGCAACTCC-3′) were used to amplify *SHN2*. Both pairs of oligonucleotides introduced *Bam*HI and *Sst*I restriction sites to the amplified fragments at their 5′ and 3′, respectively, which were used to ligate the coding region fragments to the *Bam*HI and *Sst*I sites in the pBI121 binary vector (Clontech, Palo Alto, CA) in between a 35S CaMV promoter and a nopaline synthase terminator. Oligonucleotides AP71 (5′-CAGATCTGAAGAATGGTACATTCGAAG-3′) and AP72 (5′-CTCGAGCCTTTAGACCTGTGCAATGG-3′) were used to amplify *SHN3* and introduced *Bgl*II and *Xho*I restriction sites to the amplified fragment at the 5′ and 3′, which were used to ligate the coding region fragment to the *Bam*HI and *Sal*I sites in the pNEW binary vector (a modified pBI121 binary vector, N. Marsch-Martinez, unpublished data) in between the 35S CaMV promoter and the nopaline synthase terminator. For generating the promoter:GUS constructs, fragments upstream to the ATG codon of each gene (2 kb of *SHN1/WIN1* and *SHN3* and 1.857 kb of *SHN2*) were amplified from genomic DNA (ecotype Columbia) using *Taq* DNA polymerase and oligonucleotides that introduced *Xba*I-*Nco*I restriction sites at the 5′ and 3′, respectively. Only in the case of *SHN3* did the amplified fragment already contain an endogenous *Xba*I site at the 5′ end. This allowed ligation of the fragments to the *Xba*I and *Nco*I sites in a modified pBinPlus vector (van Engelen et al., 1995; R. Greco, unpublished data) upstream of the *GUS* reporter gene. The oligonucleotides AP61 (5′-CTCTAGAACGAATGGCCGTTGATCAGAG-3′) and AP62 (5′-CCCATGGTTACTTACTCTGTG-3′) were used to amplify the *SHN1/WIN1* upstream region, AP147 (5′-CTCTAGAGATTGGGTACTAGGTTAAGG-3′) and AP148 (5′-CCCATGGTTTAGTTTCCTTCA-3′) for *SHN2* and AP149 (5′-ATCGTGTGAAACGTCAATCG-3′) and AP150 (5′-CCCATGGCTTCGAATGTACCATGGTTCTG-3′) for *SHN3*. In all cases, fragments were A-tailed and introduced to the pGEM-T Easy vector as described by the manufacturer (Promega, Madison, WI) and subsequently sequenced from both sides before digestion and ligation to the binary vector. PCR, restriction digests, plasmid DNA isolation, and gel electrophoresis were performed using standard protocols. The rd29A-DREB1A construct was similar to that described (Kasuga et al., 1999), except that the gene fusion was inserted into the pBinPlus vector. The constructs were introduced into the plants using the floral dipping transformation method (Clough and Bent, 1998). The seeds were plated on half-strength MS medium (Duchefa, Haarlem, The Netherlands) and 1% sucrose. Seedlings selected on 50 mg/L of kanamycin were subsequently transferred to the greenhouse.

### Gene Expression Analyses

Total RNA for RT-PCR was isolated from mature green rosette leaves derived from 4-week-old *shn* activation tag mutant and wild-type (ecotype Ws) plants using the Trizol reagent as described by the manufacturer (Invitrogen, Life technologies, Carlsbad, CA). Approximately 1 μg of total RNA was used for DNase I treatment and cDNA synthesis (using SuperScriptII reverse transcriptase) as described by the supplier (Invitrogen). The cDNA was diluted 50 times and used for amplification using specific oligonucleotides for the actin gene (RACTP1, 5′-GCGGTTTTCCCCAGTGTTGTTG-3′, and RACTP2, 5′-TGCCTGGACCTGCTTCATCATACT-3′) to equalize the concentrations of the cDNA samples. Subsequently, the diluted cDNA was used to perform a PCR reaction using specific oligonucleotides designed to amplify the two genes flanking the insertion site. Oligonucleotides AP8 (5′-CAAACGCTCAAGGGTCTCGTC-3′) and AP9 (5′-CTGAGCACAACCAAGTCCACCA-3′) were used to amplify the At1g15350 gene and AP6 (5′-CTTCATCGCTCTCTTCCATCC-3′) and AP7 (5′-CCAATACTTCTTCTCTGCTGC-3′) to amplify At1g15360 (*SHN1/WIN1*). The reaction conditions for PCR included a denaturing step of 95°C for 3 min, followed by 35 cycles of 1 min at 95°C, 1 min at 55°C, and 1.5 min at 72°C, ending with an elongation step of 5 min at 72°C. For the control PCR with actin oligonucleotides, 30 amplification cycles were used.

### Wax Extraction and Chemical Analysis

Cuticular wax was extracted exhaustively by dipping intact leaves twice for 30 s into 20 mL of chloroform (>99%; Fisher Scientific, Nepean, Ontario, Canada) at room temperature. Tetracosane ($C_{24}$; Sigma-Aldrich, Oakville, Ontario, Canada) was added as internal standard, the extracts were filtered, and the solvent was removed by a gentle stream of $N_2$ while heating the solution to 50°C. Then all samples were treated with bis-*N,N*-(trimethylsilyl)trifluoroacetamide (Sigma-Aldrich) in pyridine (Fluka, Buchs, Switzerland; 30 min at 70°C) to transform all hydroxyl-containing compounds into the corresponding trimethylsilyl derivatives. The

extracted surface area was subsequently measured digitally by scanning photocopies of the leaves. The qualitative composition was studied with capillary gas chromatography (GC) (6890N; Agilent, Palo Alto, CA) with He carrier gas inlet pressure constant at 30 kPa and mass spectrometric detector (70 eV, mass-to-charge ratio 50 to 750, 5973N; Agilent). GC was performed with temperature-programmed injection at 50°C oven for 2 min at 50°C, raised by 40°C·min$^{-1}$ to 200°C, held for 2 min at 200°C, then raised again by 3°C·min$^{-1}$ to 320°C and held for 30 min at 320°C. The quantitative composition of the mixtures was studied by capillary GC (Agilent; 30 m HP-1, 0.32-mm i.d., $df = 1$ μm) and flame ionization detection under the same GC conditions as above but $H_2$ carrier gas inlet pressure was programmed for 50 kPa at injection, held for 5 min, then raised with 3 kPa·min$^{-1}$ to 150 kPa and held for 40 min at 150 kPa. Single compounds were quantified against the internal standard by manually integrating peak areas.

### Chlorophyll Leaching Assay, Fresh Weight, and Stomata Analyses

For chlorophyll leaching assays, roots and inflorescence stems of 4-week-old plants were cut off, and the remaining rosette was rinsed with tap water, weighed, and put in tubes containing 30 mL of 80% ethanol at room temperature (gently agitating in the dark). Four hundred microliters were removed from each sample every 10 min during the first hour and then after 90 and 120 min. Absorbance of each sample was measured at 664 and 647, and the following formula (Lolle et al., 1997) was used to calculate the micromolar concentration of total chlorophyll per gram of fresh weight of tissue: total micromoles chlorophyll = 7.93 ($A_{664}$) + 19.53 ($A_{647}$).

Seed from the wild type and the mutant lines were stratified in cold (4°C) for three nights and sown in 9-cm diameter pots, at a density of ~12 seeds/pot. The plants were given nutrition on the 10th day after germination, allowed to grow to 4 weeks, and then used for water-loss analysis. The rosette and emerging stems of plants were detached from the roots and weighed immediately for the fresh weight. All samples maintained at room temperature (22°C) were weighed at several regular time intervals. Initial observations were taken at short time intervals of 2 min and then later gradually increased to longer intervals of 1 h. The samples were weighed for 7 h or more. Observations were taken from four different plants of wild type and mutants, and the experiment was repeated in three batches at different days. The average fresh weight, average dry weight (samples were kept at 60°C for 2 d and then weighed), average rate of water loss per unit fresh weight, and the standard deviation were calculated. A graph was plotted with average rate of water loss per unit fresh weight against time in minutes.

For stomatal density, pavement cell density and stomatal index measurements, we used similar size and age mature green rosette leaves, derived from 6-week-old plants of the wild type and 35S:*SHN1/WIN1* line no. 2-2. Two leaves from four different plants (from each of the two genotypes) were used to generate imprints of their abaxial surface. A xylene-thermocol mixture made by dissolving thermocol in xylene until the solution becomes viscous was applied uniformly on the abaxial surface of the leaves and allowed to dry. Subsequently, the imprints were detached from the leaf surface, and pieces derived from the region in between the main vein and the leaf blade edge were mounted on glass microscope slides with 50% glycerol and observed under 20× magnification using a light microscope (Zeiss, Jena, Germany). Numbers of epidermal pavement cells and stomata were counted per mm$^2$ (two different regions per leaf) and stomatal index was calculated (Mishra, 1997).

### GUS Staining and Microscopy

Tissues from various organs either from soil-grown plants or seedlings grown on half-strength MS in vitro were analyzed for their GUS expression patterns. The GUS solution contained 100 mM sodium phosphate buffer, pH 7.0, 0.5 mg/mL of 5-bromo-4-chloro-3-indolyl β-D-glucoronic acid (Duchefa), 0.1% Triton, and 0.5 mM each of potassium ferri/ferrocyanide. Samples were vacuum infiltrated and incubated at 37°C for 16 to 24 h and depleted from chlorophyll in 70% ethanol. Observation was conducted either under the binocular (WILD M3Z of Heerbrugg, Switzerland, type-S) or with a light microscope (Zeiss), and an RS Photometrics CoolSNAP camera (MediaCybernetics, Carlsbad, CA) was used to take the digital images, with the corresponding CoolSNAP software.

For scanning electron microscopy, samples were glued on a sample holder with conductive carbon cement (Leit-C; Neubauer Chemicalien, Münster, Germany) and subsequently frozen in liquid nitrogen. The samples were transferred under vacuum to a dedicated cryopreparation chamber (Oxford cryosystem, CT 1500 HF; Eynsham, UK) onto a sample stage at −90°C. Cryofractures were made at ~150°C using a cold (−196°C) scalpel blade. The fractured samples were freeze dried for 3 min at −90°C in vacuum ($3 \times 10^{-7}$ Pa) to remove water vapor contamination. After the sample surface was sputter coated with 10 nm platinum, it was transferred to the cold sample stage (−190°C) inside the Cryo-FESEM (JEOL 6300F field emission scanning electron microscope; Japan, Tokyo) and subsequently analyzed with an accelerating voltage of 5 kV. Images were digitally recorded (Orion, Brussels, Belgium).

Sequence data from this article have been deposited with the EMBL/GenBank data libraries under accession numbers BAD15859 and AAL75809.

## ACKNOWLEDGMENTS

We thank Nayelli Marsch-Martinez, Raffaella Greco, and Aarti Karaba for helpful discussions, Stephan Knapek, Stefanie Full, Sherry Wu, Charistian Landmann, and Markus Griezer along with Wim Dirkse, John Franken, and Stefan de-Folter for technical assistance, and Adrian van-Elst for assistance with scanning electron microscopy analysis. We gratefully acknowledge the use of the construct rd29A-DREB1A from Kazuo Shinozaki. This work was supported by the Center for Biosystems Genomics, Wageningen, The Netherlands.

Received March 24, 2004; accepted May 11, 2004.

## REFERENCES

**Aarts, M.G.M., Keijzer, C.J., Stiekema, W.J., and Pereira, A.** (1995). Molecular characterization of the CER1 gene of Arabidopsis involved in epicuticular wax biosynthesis and pollen fertility. Plant Cell **7,** 2115–2127.

**Alonso, J.M., et al.** (2003). Genome-wide insertional mutagenesis of *Arabidopsis thaliana*. Science **301,** 653–657.

**Altschul, S.F., Gish, W., Miller, W., Myers, E.W., and Lipman, D.J.** (1990). Basic local alignment search tool. J. Mol. Biol. **215,** 403–410.

**Bird, S.M., and Gray, J.E.** (2003). Signals from the cuticle affect epidermal cell differentiation. New Phytol. **157,** 9–23.

**Blee, E., and Schuber, F.** (1993). Biosynthesis of cutin monomers: Involvement of a lipoxygenase/peroxygenase pathway. Plant J. **4,** 113–123.

**Chen, W., et al.** (2002). Expression profile matrix of Arabidopsis transcription factor genes implies their putative functions in response to environmental stresses. Plant Cell **14,** 559–574.

**Chen, X., Goodwin, S.M., Boroff, V.L., Liu, X., and Jenks, M.A.** (2003). Cloning and characterization of the *WAX2* gene of Arabidopsis

involved in cuticle membrane and wax production. Plant Cell **15,** 1170–1185.

**Clough, S.J., and Bent, A.F.** (1998). Floral dip: A simplified method for Agrobacterium-mediated transformation of *Arabidopsis thaliana*. Plant J. **16,** 735–743.

**Fiebig, A., Mayfield, J.A., Miley, N.L., Chau, S., Fischer, R.L., and Preuss, D.** (2000). Alterations in *CER6*, a gene identical to *CUT1*, differentially affect long-chain lipid content on the surface of pollen and stems. Plant Cell **12,** 2001–2008.

**Gray, J.E., Holroyd, G.H., van der Lee, F.M., Bahrami, A.R., Sijmons, P.C., Woodward, F.I., Schuch, W., and Hetherington, A.M.** (2000). The HIC signalling pathway links CO2 perception to stomatal development. Nature **408,** 713–716.

**Hooker, T.S., Millar, A.A., and Kunst, L.** (2002). Significance of the expression of the *CER6* condensing enzyme for cuticular wax production in Arabidopsis. Plant Physiol. **129,** 1568–1580.

**James, D.W., Jr., Lim, E., Keller, J., Plooy, I., Ralston, E., and Dooner, H.K.** (1995). Directed tagging of the Arabidopsis *FATTY ACID ELONGATION1* (*FAE1*) gene with the maize transposon *Activator*. Plant Cell **7,** 309–319.

**Jenks, M.A., Eigenbrode, S.D., and Lemeiux, B.** (2002). Cuticular waxes of Arabidopsis. In The Arabidopsis Book, C.R. Somerville and E.M. Meyerowitz, eds (Rockville, MD: American Society of Plant Biologists), doi/10.1199/tab.0016, http://www.aspb.org/publications/arabidopsis/.

**Jenks, M.A., Rashotte, A.M., Tuttle, H.A., and Feldmann, K.A.** (1996). Mutants in Arabidopsis thaliana altered in epicuticular wax and leaf morphology. Plant Physiol. **110,** 377–385.

**Jetter, R., and Schaffer, S.** (2001). Chemical composition of the *Prunus laurocerasus* leaf surface. Dynamic changes of the epicuticular wax film during leaf development. Plant Physiol. **126,** 1725–1737.

**Kasuga, M., Liu, Q., Miura, S., Yamaguchi-Shinozaki, K., and Shinozaki, K.** (1999). Improving plant drought, salt, and freezing tolerance by gene transfer of a single stress-inducible transcription factor. Nat. Biotech. **17,** 287–291.

**Kolattukudy, P.E.** (1981). Structure, biosynthesis and biodegradation of cutin and suberin. Annu. Rev. Plant Physiol. **32,** 539–567.

**Koornneef, M., Hanhart, C.J., and Thiel, F.** (1989). A genetic and phenotypic description of *eceriferum* (*cer*) mutants of *Arabidopsis thaliana*. J. Hered. **80,** 118–122.

**Krolikowski, K.A., Victor, J.L., Wagler, T.N., Lolle, S.J., and Pruitt, R.E.** (2003). Isolation and characterization of the Arabidopsis organ fusion gene *HOTHEAD*. Plant J. **35,** 501–511.

**Kumar, G.N.M., and Knowles, N.R.** (2003). Wound-induced superoxide production and PAL activity decline with potato tuber age and wound healing ability. Physiol. Plant. **117,** 108–117.

**Kunst, L., and Samuels, A.L.** (2003). Biosynthesis and secretion of plant cuticular wax. Prog. Lipid Res. **42,** 51–80.

**Kurata, T., Kawabata, A.C., Sakuradani, E., Shimizu, S., Okada, K., and Wada, T.** (2003). The *yore-yore* gene regulates multiple aspects of epidermal cell differentiation in Arabidopsis. Plant J. **36,** 55–66.

**Le-Bouquin, R., Skrabs, M., Kahn, R., Benveniste, I., Salaun, J.P., Schreiber, L., Durst, F., and Pinot, F.** (2001). CYP94A5, a new cytochrome P450 from Nicotiana tabacum is able to catalyze the oxidation of fatty acids to the omega-alcohol and to the corresponding diacid. Eur. J. Biochem. **268,** 3083–3090.

**Liu, Q., Kasuga, M., Sakuma, Y., Abe, H., Miura, S., Yamaguchi, S.K., and Shinozaki, K.** (1998). Two transcription factors, DREB1 and DREB2, with an EREBP/AP2 DNA binding domain separate two cellular signal transduction pathways in drought-and low-temperature-responsive gene expression, respectively, in Arabidopsis. Plant Cell **10,** 1391–1406.

**Lolle, S.J., Berlyn, G.P., Engstrom, E.M., Krolikowski, K.A., Reiter Wolf, D., and Pruitt, R.E.** (1997). Developmental regulation of cell interactions in the Arabidopsis *fiddlehead-1* mutant: A role for the epidermal cell wall and cuticle. Dev. Biol. **189,** 311–321.

**Lolle, S.J., Hsu, W., and Pruitt, R.E.** (1998). Genetic analysis of organ fusion in *Arabidopsis thaliana*. Genetics **149,** 607–619.

**Marsch-Martinez, N., Greco, R., van-Arkel, G., Herrera-Estrella, L., and Pereira, A.** (2002). Activation tagging using the En-I maize transposon system in Arabidopsis. Plant Physiol. **129,** 1544–1556.

**McNevin, J.P., Woodward, W., Hannoufa, A., Feldmann, K.A., and Lemieux, B.** (1993). Isolation and characterization of eceriferum (cer) mutants induced by T-DNA insertions in *Arabidopsis thaliana*. Genome **36,** 610–618.

**Memelink, J., Verpoorte, R., and Kijne, J.W.** (2001). ORCAnization of jasmonate-responsive gene expression in alkaloid metabolism. Trends Plant Sci. **6,** 212–219.

**Millar, A.A., Clemens, S., Zachgo, S., Giblin, E.M., Taylor, D.C., and Kunst, L.** (1999). *CUT1*, an Arabidopsis gene required for cuticular wax biosynthesis and pollen fertility, encodes a very-long-chain fatty acid condensing enzyme. Plant Cell **11,** 825–838.

**Millar, A.A., and Kunst, L.** (1997). Very-long-chain fatty acid biosynthesis is controlled through the expression and specificity of the condensing enzyme. Plant J. **12,** 121–131.

**Mishra, M.K.** (1997). Stomatal characteristics at different ploidy levels in *Coffea L*. Ann. Bot. **80,** 689–692.

**Moire, L., Schmutz, A., Buchala, A., Yan, B., Stark, R., and Ryser, U.** (1999). Glycerol is a suberin monomer. New experimental evidence for an old hypothesis. Plant Physiol. **9,** 1137–1146.

**Nakazawa, M., Ichikawa, T., Ishikawa, A., Kobayashi, H., Tsuhara, Y., Kawashima, M., Suzuki, K., Muto, S., and Matsui, M.** (2003). Activation tagging, a novel tool to dissect the functions of a gene family. Plant J. **34,** 741–750.

**Nawrath, C.** (2002). The biopolymers cutin and suberin. In The Arabidopsis Book, C.R. Somerville and E.M. Meyerowitz, eds (Rockville, MD: American Society of Plant Biologists), doi/10.1199/tab.0021, http://www.aspb.org/publications/arabidopsis/.

**Negruk, V., Yang, P., Subramanian, M., McNevin John, P., and Lemieux, B.** (1996). Molecular cloning and characterization of the CER2 gene of Arabidopsis thaliana. Plant J. **9,** 137–145.

**Nicholas, K.B., Nicholas, H.B., Jr., and Deerfield, D.W.** (1997). GeneDoc: Analysis and visualization of genetic variation. EMBNET News **4,** 1–4.

**Okamuro, J.K., Caster, B., Villarroel, R., Van Montagu, M., and Jofuku, K.D.** (1997). The AP2 domain of APETALA2 defines a large new family of DNA binding proteins in Arabidopsis. Proc. Natl. Acad. Sci. USA **94,** 7076–7081.

**Page, R.D.M.** (1996). TREEVIEW: An application to display phylogenetic trees on personal computers. Comput. Appl. Biosci. **12,** 357–358.

**Pereira, A., and Aarts, M.G.M.** (1998). Transposon Tagging with the En-I System. (Totowa, NJ: Humana Press).

**Pruitt, R.E., Vielle-Calzada, J.P., Ploense, S.E., Grossniklaus, U., and Lolle, S.J.** (2000). *FIDDLEHEAD*, a gene required to suppress epidermal cell interactions in Arabidopsis, encodes a putative lipid biosynthetic enzyme. Proc. Natl. Acad. Sci. USA **97,** 1311–1316.

**Reina, J.J., and Heredia, A.** (2001). Plant cutin biosynthesis: The involvement of a new acyltransferase. Trends Plant Sci. **6,** 296.

**Riechmann, J.L., and Meyerowitz, E.M.** (1998). The AP2/EREBP family of plant transcription factors. Biol. Chem. **379,** 633–646.

**Roberts, J.A., Elliott, K.A., and Gonzalez-Carranza, Z.H.** (2002). Abscission, dehiscence, and other cell separation processes. Annu. Rev. Plant Biol. **53,** 131–158.

**Roberts, J.A., Whitelaw, C.A., Gonzalez-Carranza, Z.H., and McManus, M.T.** (2000). Cell separation processes in plants: Models, mechanisms and manipulation. Ann. Bot. **86,** 223–235.

**Sanders, P.M., Bui, A.Q., Weterings, K., McIntire, K.N., Hsu, Y.C., Lee, P.Y., Truong, M.T., Beals, T.P., and Goldberg, R.B.** (1999). Anther developmental defects in Arabidopsis thaliana male-sterile mutants. Sex. Plant Reprod. **11,** 297–322.

**Schnurr, J., Shockey, J., and Browse, J.** (2004). The Acyl-CoA synthetase encoded by *LACS2* is essential for normal cuticle development in Arabidopsis. Plant Cell **16,** 629–642.

**Schreiber, L., Hartmann, K., Skrabs, M., and Zeier, J.** (1999). Apoplastic barriers in roots: Chemical composition of endodermal and hypodermal cell walls. J. Exp. Bot. **50,** 1267–1280.

**Shuai, B., Reynaga, P.C.G., and Springer, P.S.** (2002). The *LATERAL ORGAN BOUNDARIES* gene defines a novel, plant-specific gene family. Plant Physiol. **129,** 747–761.

**Sieber, P., Schorderet, M., Ryser, U., Buchala, A., Kolattukudy, P., Metraux, J.P., and Nawrath, C.** (2000). Transgenic Arabidopsis plants expressing a fungal cutinase show alterations in the structure and properties of the cuticle and postgenital organ fusions. Plant Cell **12,** 721–737.

**Singh, K., Foley, R.C., and Onate-Sanchez, L.** (2002). Transcription factors in plant defense and stress responses. Curr. Opin. Plant Biol. **5,** 430–436.

**Smyth, D.R., Bowman, J.L., and Meyerowitz, E.M.** (1990). Early flower development in Arabidopsis. Plant Cell **2,** 755–767.

**Tanaka, H., Onouchi, H., Kondo, M., Hara-Nishimura, I., Nishimura, M., Machida, C., and Machida, Y.** (2001). A subtilisin-like serine protease is required for epidermal surface formation in Arabidopsis embryos and juvenile plants. Development **128,** 4681–4689.

**Thompson, J.D., Gibson, T.J., Plewniak, F., Jeanmougin, F., and Higgins, D.G.** (1997). The CLUSTAL-X windows interface: Flexible strategies for multiple sequence alignment aided by quality analysis tools. Nucleic Acids Res. **25,** 4876–4882.

**Todd, J., Post-Beittenmiller, D., and Jaworski, J.G.** (1999). *KCS1* encodes a fatty acid elongase 3-ketoacyl-CoA synthase affecting wax biosynthesis in *Arabidopsis thaliana*. Plant J. **17,** 119–130.

**van Engelen, F.A., Molthoff, J.W., Conner, A.J., Nap, J.P., Pereira, A., and Stiekema, W.J.** (1995). pBINPLUS: An improved plant transformation vector based on pBIN19. Transgenic Res. **4,** 288–290.

**Wellesen, K., Durst, F., Pinot, F., Benveniste, I., Nettesheim, K., Wisman, E., Steiner-Lange, S., Saedler, H., and Yephremov, A.** (2001). Functional analysis of the *LACERATA* gene of Arabidopsis provides evidence for different roles of fatty acid omega-hydroxylation in development. Proc. Natl. Acad. Sci. USA **98,** 9694–9699.

**Xia, Y., Nikolau, B.J., and Schnable, P.S.** (1996). Cloning and characterization of *CER2*, an Arabidopsis gene that affects cuticular wax accumulation. Plant Cell **8,** 1291–1304.

**Yephremov, A., Wisman, E., Huijser, P., Huijser, C., Wellesen, K., and Saedler, H.** (1999). Characterization of the *FIDDLEHEAD* gene of Arabidopsis reveals a link between adhesion response and cell differentiation in the epidermis. Plant Cell **11,** 2187–2201.

**Yoshida, R., Hobo, T., Ichimura, K., Mizoguchi, T., Takahashi, F., Aronso, J., Ecker, J.R., and Shinozaki, K.** (2002). ABA-activated SnRK2 protein kinase is required for dehydration stress signaling in Arabidopsis. Plant Cell Physiol. **43,** 1473–1483.

**Zimmermann, H.M., Hartmann, K., Schreiber, L., and Steudle, E.** (2000). Chemical composition of apoplastic transport barriers in relation to radial hydraulic conductivity of corn roots (*Zea mays L.*). Planta **210,** 302–311.

## NOTE ADDED IN PROOF

Another similar study was recently published in PNAS.

**Broun, P., Poindexter, P., Osborne, E., Jiang, C., and Riechmann, J.L.** (2004). WIN1, a transcriptional activator of epidermal wax accumulation in Arabidopsis. Proc. Natl. Acad. Sci. USA **101,** 4706–4711.